ABDULRRAHMAN A. DAKHIL

EXPERIMENTAL ANALYSIS OF THE BEHAVIOR OF COMPOSITE COLUMN-REINFORCED CONCRETE BEAM JOINTS

THE GRADUATE SCHOOL OF NATURAL AND APPLIED SCIENCES
OF
ATILIM UNIVERSITY

ABDULRRAHMAN A. DAKHIL

A MASTER OF SCIENCE THESIS
IN
THE DEPARTMENT OF CIVIL ENGINEERING

AUGUST 2020

ATILIM UNIVERSITY 2020

EXPERIMENTAL ANALYSIS OF THE BEHAVIOR OF COMPOSITE COLUMN-REINFORCED CONCRETE BEAM JOINTS

A THESIS SUBMITTED TO
THE GRADUATE SCHOOL OF NATURAL AND APPLIED SCIENCES
OF
ATILIM UNIVERSITY

BY

ABDULRRAHMAN A. DAKHIL

IN PARTIAL FULFILLMENT OF THE REQUIREMENTS
FOR
THE DEGREE OF MASTER OF SCIENCE
IN
THE DEPARTMENT OF CIVIL ENGINEERING

AUGUST 2020

Approval of the Graduate School of Natural and Applied Sciences, Atilim University.

_____

Prof. Dr. Ali KARA
Director

I certify that this thesis satisfies all the requirements as a thesis for the degree of **Master of Science in Civil Engineering Department, Atilim University**.

_____

Prof. Dr. Hasan Umur AKAY
Head of Department

This is to certify that we have read the thesis EXPERIMENTAL ANALYSIS OF THE BEHAVIOR OF COMPOSITE COLUMN-REINFORCED CONCRETE BEAM JOINTS submitted by ABDULRRAHMAN DAKHIL and that in our opinion it is fully adequate, in scope and quality, as a thesis for the degree of Master of Science.

_____	_____
Asst. Prof. Dr. Halit Cenan MERTOL Co-Supervisor	Asst. Prof. Dr. Gökhan TUNÇ Supervisor

Examining Committee Members:

Prof.Dr. Eray Baran
Civil Eng. Department, METU _____

Assist. Prof. Dr. Gökhan Tunç
Civil Eng. Department, Atilim University _____

Assist. Prof. Dr. Halit Cenan Mertol
Civil Eng. Department, Atilim University _____

Prof.Dr. Tolga Akış
Civil Eng. Department, Atilim University _____

Assist. Prof. Dr. Ertan Sönmez
Civil Eng. Department, Atilim University _____

Date: *August 5, 2020*

I hereby declare that all information in this document has been obtained and presented in accordance with academic rules and ethical conduct. I also declare that, as required by these rules and conduct, I have fully cited and referenced all material and results that are not original to this work.

Name, Last Name: ABDULRRAHMAN A. DAKHIL

Signature:

ABSTRACT

EXPERIMENTAL ANALYSIS OF THE BEHAVIOR OF COMPOSITE COLUMN-REINFORCED CONCRETE BEAM JOINTS

Dakhil, Abdulrrahman

M.S., Department of Civil Engineering

Supervisor: Asst. Prof. Dr. Gökhan Tunç

Co-Supervisor: Asst. Prof. Dr. Halit Cenan Mertol

August 2020, 63 pages

This thesis is dedicated to improving our understanding and assessment of the seismic efficiency and vulnerability of the SRC column to RC beam joints in composites, and their ability to dissipate seismic energy through inelastic deformations. In this study, experimental aspects regarding the seismic performance of high ductility and low ductility steel-concrete composite frame were investigated. A literature review was performed, leading to the development of a new column-beam joint. The basic design parameter in this study was ductility, which is considered a conceptual framework in Efficiency-Base Seismic Engineering. Thus, attention was focused on assuring various ductility ranges of composite joints, which can be all obtained through a detailed study of the Turkish Earthquake Code (TEC 18). After identifying deficiencies and the energy dissipation capacity in the new proposed joints, two half scaled frames with specific ductility related designs were built, instrumented, tested, and analyzed. The specimens were tested under displacement-controlled lateral cyclic loading that incorporated constant axial loading to create cyclic tension and compression facets across the joint area. The test parameters were column reinforcement ratios, joint aspect ratios, axial loads, and cyclic lateral loads. The test results proved that the SRC column–RC beam frames, employing an extra column reinforcement ratio, exhibit better seismic performance.

Keywords: RC beam, SRC column, composite joint, seismic performance, structural element, ductility.

ÖZ

KOMPOZİT KOLON-BETONARME KİRİŞ BİRLEŞİM BÖLGELERİNİN DENEYSEL ANALİZLE DAVRANIŞININ BELİRLENMESİ

Dakhil, Abdulrrahman

Yüksek Lisans (M.S.), İnşaat Mühendisliği Bölümü

Tez Yöneticisi : Dr. Öğr. Üyesi Gökhan TUNÇ

Ortak Tez Yöneticisi : Dr. Öğr. Üyesi Halit Cenan MERTOL

Ağustos 2020, 63 sayfa

Bu tezde, yüksek ve sınırlı süneklik düzeylerine sahip çelik-betonarme kompozit çerçevelerin deprem performansları deneysel olarak incelenmiştir. Yapılan deneysel çalışma ile SRC kolon ve betonarme kiriş kompozit birleşim bölgelerinin depreme karşı davranış ve hasar görebilirlik özelliği ile bu birleşim bölgelerinin deprem enerjisini elastik olmayan deplasmanlar yardımı ile soğurabilme yeteneği araştırılmış ve konu detaylı olarak irdelenmiştir. Bu kapsamda, akademik kaynak taraması yapılarak kolon-kiriş bağlantısının tasarımı ve davranışı için yeni bir bakış açısı elde edilmeye çalışılmıştır. Tez çalışmasında verimlilik esasına dayalı deprem mühendisliği kavramı çerçevesinde kullanılan temel tasarım parametresi ise sünekliktir. Bu çalışma ile yürürlükteki Türkiye Bina Deprem Yönetmeliği (TBDY 2018) uyarınca detayları elde edilen kompozit kolon-kiriş bağlantılarının tasarım gereği ihtiyaç duyulan değişken süneklik taleplerine göre davranışının belirlenmesi hedeflenmiştir. Kolon-kiriş bağlantılarındaki eksikliklerin ve enerji soğurma kapasitelerinin belirlenmesini müteakip, ½ ölçek oranındaki çerçeveler belirlenen süneklik hedeflerine uygun olarak tasarlanmış, deneysel ölçüm cihazları yerleştirilerek, testleri ve analizleri gerçekleştirilmiştir. Deneylerde, bağlantı noktalarına deplasman kontrollü yatay tersinir çekme ve basınç kuvvetleri ile sabit eksenel yük uygulanmıştır. Deneysel çalışmalarda kullanılan parametreler ise şunlardır: kolon donatı oranı, bağlantı ebat oranı, eksenel yük ve yatay tersinir yükler. Yapılan deneyler neticesinde SRC kolon-betonarme kirişlerden oluşan çerçevelerde ilave kolon donatı miktarlarının deprem davranışını olumlu yönde etkilediği görülmüştür.

Anahtar Kelimeler: Betonarme kiriş, SRC kolon, kompozit birleşim bölgeleri, deprem performansı, yapısal elemanlar, süneklik.

To my family

ACKNOWLEDGMENTS

The author sincerely expresses his deepest gratitude to the Almighty. I hope He blesses this work as an ongoing charity and a beneficial knowledge for Humanity to save precious lives during future earthquakes.

First and foremost, the author would like to express his thanks to his supervisor Asst. Prof. Dr. Gökhan TUNÇ, Department of Civil Engineering, Atilim University. He has always been a tremendous mentor. His enthusiasm towards the advanced analysis of composite structures, patience, knowledge, and constructive advice has been the key to successfully complete this thesis.

The author also wishes to express his deepest gratitude to his co-supervisor Asst. Prof. Dr. Halit Cenan MERTOL, Department of Civil Engineering, Atilim University for his invaluable suggestions, motivation, and affectionate encouragement, which helped accomplish this study.

The author also takes the opportunity to pay his heartfelt thanks to staff members of Structural Engineering Laboratory Mr. Engin Alp and Mr. Dogan Tok for their consistent support and painstaking contributions to the experimental work.

The author also appreciatively remembers the assistance and encouragement of his friends and well-wishers and everyone related to carry out and complete this study.

Finally, the author wishes to express his deep gratitude to my father (Dr. Abdulmuhsen), mother (Eng. Nagat), and my siblings (Amel & Mohamed) for believing in me, their constant support, encouragement, and sacrifice throughout the research work.

TABLE OF CONTENTS

LIST OF TABLES

LIST OF FIGURES

LIST OF ABBREVIATIONS

ACI	American Concrete Institution
AISC	American Institute of Steel Construction
CFRP	Carbon Fiber Reinforced Polymer
CFST	Concrete Filled Steel Tube
CFT	Concrete Filled Tube
ESJ	Enveloped Steel Jackets
HD	High Ductile Frame
LD	Low Ductile Frame
LVDT	Linear Variable Differential Transformer
RC	Reinforced Concrete
SAP2000	Structural Analysis Program by Computers and Structures
SRC	Reinforced Concrete Encased Steel
TEC 18	2018 Turkish Earthquake Code
TS 500	Turkish Standard for the Requirements of Design and Construction of Reinforced Concrete Structures

LIST OF SYMBOLS

A_c	:	Cross-sectional area of concrete
A_g	:	Gross cross-sectional area of the column
A_s	:	Cross-sectional area of transverse reinforcement
A_{st}	:	Cross-sectional area of structural steel
f_{ck}	:	Characteristic compressive strength of concrete
h_b	:	Height of the joint core
h_c	:	Width of the joint core
n	:	Number of stirrups
N_{dm1}	:	Axial compressive strength of concrete
N_{dm2}	:	Axial compressive strength of the structural
P_n	:	Axial compressive strength of the composite column
γ_b	:	Joint shear strain at the beam side
γ_c	:	Joint shear strain at the column side
ρ	:	Transverse reinforcement ratio
ρ_a	:	Steel ratio
ρl	:	Cross-section reinforcing ratio
ρ_v	:	Stirrup ratio
σ_y	:	Yield strength of structural steel

CHAPTER 1

INTRODUCTION

This chapter concisely contains a general overview of the thesis on the experimental analysis of steel-concrete composite frame joints utilizing two scaled-down frames. Each frame is composed of two reinforced concrete-encased steel (SRC) columns and one connecting reinforced concrete (RC) beam. These frames are designed to be high ductile and low ductile frames in accordance with the TS 500, the Turkish standard for the requirements of design and construction of reinforced concrete structures, and the Turkish Earthquake Code (TEC 18).

1.1. Background on Structural Systems

The structural system is a confluence of approaches of assembling and constructing components of a building in a certain way that they can securely support and distribute loads to the ground without exceeding the allowable stress on the members. Much of the structural systems are implemented and currently in service are designed to meet several functional requirements in structures. Composite steel-concrete structures are one of those structures that are being widely used in the current construction industry; for example, modern bridges, sports stadia, medium, and high-rise buildings as well as offshore structures. This is because of their intended functions in achieving long spans, lower story heights, high strength, and high stiffness. Besides, the composite technique provides mechanical and economic benefits.

1.1.1 Reinforced concrete structural systems

Reinforced concrete structure refers to elements like beams, columns, slabs consisting of steel bars encased by concrete. Generally, concrete is the most common construction material. Simply, this is due to its relatively high compressive strength, ingrained stiffness, fire resistance, corrosion resistance, long life, and low erection costs as well

as ease of casting regardless of the shape and size needed. Characteristics such as strength, setting time, fire resistance, and workability of the concrete might be improved employing several sorts of cement and chemical additives. However, concrete might show several drawbacks including low tensile strength, slow erect and heavyweight as well as its general failure due to cracking and crushing.

1.1.2 Steel structural systems

Structured steel frames refer to building frame systems where the vertical and horizontal fixed elements are formed by structural steel beams and columns. Structural steel has a couple of advantages like strength, durability, light in weight, easy installation and speed in construction, versatile, easy fabrication in different sizes, and most significant ductility. Nonetheless, steel has some drawbacks like high maintenance, capital cost, susceptibility to buckling, fatigue, fracture, and fire damage.

1.1.3 Composite structural systems

The composite structural system refers basically to structural elements that are made up of two or more dissimilar materials. These systems are commonly implemented in reinforced concrete buildings in the form of composite columns, beams, and joists. When structural steel and reinforced concrete appropriately integrated, they can produce synergetic savings in initial and life-cycle costs. Besides, composite frame imposes enhanced structural capabilities such as large load carrying capacity, high ductility in seismic active zones, ingrained stiffness which decreases the building drift ratio. Moreover, it has high damping characteristics combined with inherent advantages in areas of fire protection, corrosion resistance, construction techniques, and reduction in cross-sectional area of the elements that have verified to be a reasonably priced choice for designers.

Nowadays, great incremental use of composite materials has been perceived in the construction industry. For instance, the classification of the 100 tallest buildings in the world considering the use of construction material from 1930 to 2016 is illustrated in Figure 1.1. It is evident that there is a gradual decrease in steel-based construction afterward in 1960. On the other hand, the use of composite steel-concrete construction

in tall buildings has increased gradually from 12% to 53%; in particular from 1980 to 2016. This emphasizes the scope of utilizing composite structures in the construction industry.

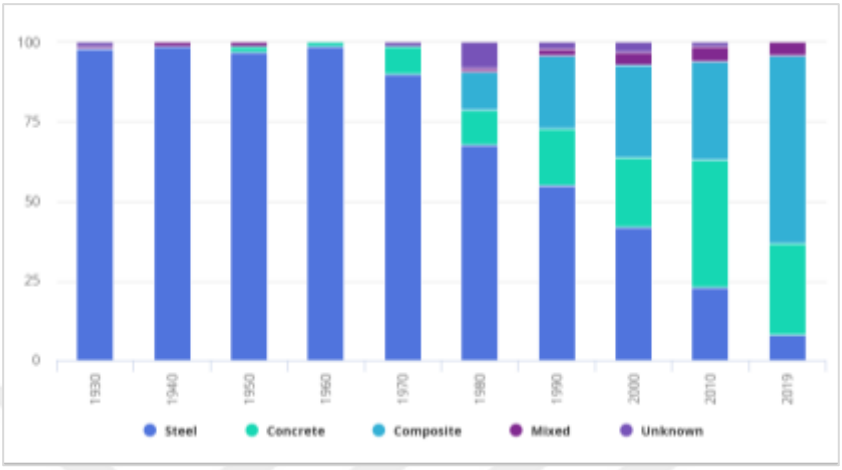

Figure 1.1 World's 100 tallest building by material [1]

As with most composite construction, the beam-column connection is of special concern. It is basically the most dominant component not only in assuring the structural integrated performance of the system but also in the issue of strain compatibility between the steel and concrete under the introduction of seismic loading. Earthquake reconnaissance has shown substantial vulnerability and structural damage that can result from the inadequacy of beam-column joint design considerations. Since the 1960s, great efforts have been dedicated to improving the adequate seismic performance of those joints. In spite of all these tremendous revisions to improve new design concepts, very limited efforts have been accomplished in understanding the performance of composite joints compromising of reinforced concrete-encased steel (SRC) columns and reinforced concrete (RC) beams designed as seismically resistant.

1.2. Problem Statement

Modern codes such as TS 500 and Turkish Earthquake Code, TEC 18, for buildings in seismically active areas allow the design of high ductile and low ductile systems and also provide designers with certain building regulations, taking into account the fulfillment of intended ductility. In the existing codes; however, there is no specific

provision for the design of composite structures. Consequently, for making up this lack, a new steel-concrete composite joint has been suggested. The verification of its ductility will be quantified at the same level as the strength and the stiffness; then, a set of recommendations will be addressed.

Moreover, the available literature concerning the seismic behavior of the confined composite beam-column joints is relatively limited. For instance, scarce experimental investigations have been done concerning the seismic performance of the SRC column with RC beam joints, and accordingly not much data has been published regarding this issue. Furthermore, there is a lack of accuracy in those studies that address the realistic conditions of structures such as a realistic axial load level. In fact, very few studies were focused on testing this type of joints under their realistic conditions because of the associated testing complications. The potential axial and shear failure of this type of joints is also unidentified. As a result, a profound experimental investigation is required for addressing these shortages. It should be noted that among the types of composite columns and beams, this thesis focuses on square SRC columns with headed shear studs and RC beams.

1.3. Purpose of Study

This study is aiming at filling unresolved voids in understanding and evaluating the seismic efficiency and vulnerability of the SRC column to RC beam joints in composite structures. As such, to achieve this aim a set of specific objectives of this research can be summarized as follows:

1. Conducting a comprehensive literature review on available tests and theoretical models attributed to the seismic efficiency of the confined beam-column joints.
2. Estimating the primary parameters and essential failure modes in the seismic performance of confined beam-column joints.
3. Analyzing experimentally the effect of cyclic lateral loads on the resilience and deformability of joints through realistically designed tests.
4. Identifying the effect of column reinforcement ratio on seismic efficiency of confined beam-column joints.

5. Carrying out a comparative study between high and low ductile composite frames with SRC columns.
6. Serve as a reference for calibrating and evaluating joint shear strength and axial efficiency models (for future works).

1.4. Scope of Study

The experimental program consisted of two frames with a concrete-encased steel SRC column to RC beam joints. The scale factor of 1:2 was chosen to reveal the actual behavior of the composite joints in the industrial application. A total of two frames were designed according to the different engineering requirements. For instance, the percentages of structural steel were 2.45% and 4.46% in these columns because one of these frames was constructed as high ductile and the other one was constructed as low ductile, respectively. These frames; however, had the same normal strength concrete 30 MPa, yield strength of reinforcement steel is 428 MPa and strength of the structural steel 317 MPa. The frames were tested under the combined action of a constant axial load and reversed cyclic lateral displacements simultaneously.

1.5. Thesis Outline

In this thesis study, two experimental models of steel-reinforced concrete beam-to-column connections are erected considering different ductility parameters. Models are then verified through the axial and lateral testing. This thesis is organized into 5 chapters:

Chapter 1 provides brief information on composite structures and their behavior under earthquake loading. The thesis problem statement, objectives, and scope of the study are presented in this chapter. Chapter 2 provides a brief overview of the literature on the SRC column to RC beam joints and summarizes the experimental and theoretical work conducted on it. Chapter 3 introduces the experimental program of the composite frame along with its parameters that would be examined. It also provides an overview of the fabrication process of all structural members and concrete pouring. A detailed description of the test setups including fixtures, instrumentation, and

loading condition is also included in Chapter 3. Chapter 4 includes experimental results and observations. Chapter 5 provides the conclusions of this research work and some recommendations for future works.

CHAPTER 2

LITERATURE REVIEW

A literature review was conducted on the seismic performance of reinforced concrete-encased steel (SRC) column and reinforced concrete (RC) beam joints. Recent and past analytical and experimental studies related to these joints that have been performed by different researchers were covered as well. The foundation of the study was established through a detailed literature review of many articles and publications relating to different aspects of the study. An investigation of relevant publications, citations, and references was carried out using multiple databases available in the library databases of Atilim University. Different tests were carried out on frames with distinctive layout configurations, setups, and scales. Most of those testing frames were built up with normal strength concrete subjected to multiple cyclic concentric, eccentric and biaxial loads. The findings of these investigations were briefly discussed below:

Peng et al. (2019) have conducted a research work on the seismic behavior of reinforced concrete (RC) beam and steel-reinforced concrete (SRC) column composite connection. In this study, the joint region was enhanced in terms of its strength with carbon fiber reinforced polymer (CFRP) sheets and enveloped steel jackets (ESJ). The objective of this study was to define the impact of the containment materials and degree of damage on the seismic behavior of the RC beam-SRC column composite joints. Based on the Chinese Seismic Design Code (GB 50011-2010), nine SRC frame joints were designed and constructed on a scale of 1:2 to simulate pre-damage loading. The beam layout configuration area was 200 mm by 320 mm, while the column interface was 250 mm by 250 mm. In the core region of the joint specimen, a column-through type was used. The thickness of both of the stiffener and the connecting plate welded with section steel was 5 mm, thickness the specimen's protective covering was 20 mm, and the effective height of the frame joint was 1,570 mm. The concrete cube's mean value of the compressive strength measured was 38.8 MPa. The test was

conducted to simulate the pre-damage load that is a rehabilitation process that was done mostly either with carbon fiber reinforced polymer sheets or enveloped steel jackets. After the rehabilitation process, a lateral cyclic load destruction test was conducted to evaluate the performance of the two reinforcement materials (CFRP sheets and ESJ) for varying levels of seismic damage. As a part of the discussion, an evaluation of the bearing capacity degradation, skeleton curves, energy dissipation, ductility, hysteretic curves, stiffness degradation, and strain-displacement curves of the tested samples demonstrated good reinforcement efficiency of the two strengthening materials [2].

Besides, the enveloped steel jackets improved the specimen's rigidity and bearing capability, and the carbon fiber reinforced polymer sheets enhanced the ductility and energy dissipation of the specimen, thereby improving the specimen's seismic performance. Thus, the significantly damaged specimen reinforced with CFRP sheets or ESJ did not collapse in a simulated drastic earthquake and was nearly identical to or exceeded the original specimen's seismic performance. Likewise, for the ESJ reinforced sample, the ductility and dissipation of energy were lower than that of the CFRP-strengthened specimen. The ESJ material would be therefore preferable if only one type of material to be used in reinforcing the specimen. Furthermore, the seismic performance of the RC beam-SRC column frame joints strengthened with the CFRP sheets and ESJ was simulated using a finite element analysis software ABAQUS [3]. Eventually, the results obtained from experimental work were in accord with those obtained through simulation. In other words, it has been proven that there was a quite consonance between the simulated and experimental results of the ultimate joint capacity in the core zones. This complied with the design principle of "strong joint, weak member" [2].

Similarly, in 2019, Ma et al. have investigated the seismic performance of the concrete-encased steel tubular (CFST) column to reinforced concrete (RC) beam joint experimentally. The key point of this investigation was determining the response of a newly proposed joint between the steel tube and the longitudinal RC beam. Accordingly, thirteen concrete CFST columns to RC beam joints specimens

were constructed. For simulating the realistic behavior of the composite a scale ratio of 1:5 was selected. In the study, six types of joint specimens were used. These joint specimens were designed on the basis of different engineering specifications, for example, square interior joint, rectangular column interior joint, rectangular column exterior joint, staggered joint, rectangular column exterior, unsymmetrical joint, and double beam joint as shown in Figure 2.1. The system was then evaluated by applying axial load on the top of the column by a hydraulic jack and cyclic loading to the ends of the beam through four attached actuators. Multiple aspects that represent the seismic efficiency of such composite joints were analyzed such as the joint types, axial load rate, stiffness and strength degradation, ductility, energy dissipation capacity, and stress growth based on the test results. The author concluded that four kinds of joint failure modes were observed in the current test namely, beam bending-shear failure, beam bending failure, joint shear failure, and column compression-bending failure. On the other hand, dissimilar types of joints had a small impact on the strength, ductility, and the energy dissipation of the joint capacity. The author also pointed out that the CFST column type to the RC beam joint could be categorized as rigid joints with only joint shear failure mode and beam bending failure mode. Additionally, the column compression-bending failure joint had a large beam section that led to the high stiffness of the beam. This sort of joints might be categorized as semi-rigid. Moreover, the energy dissipation of this composite joint type is slightly higher than that of the CFST column as well as the RC column joint [4].

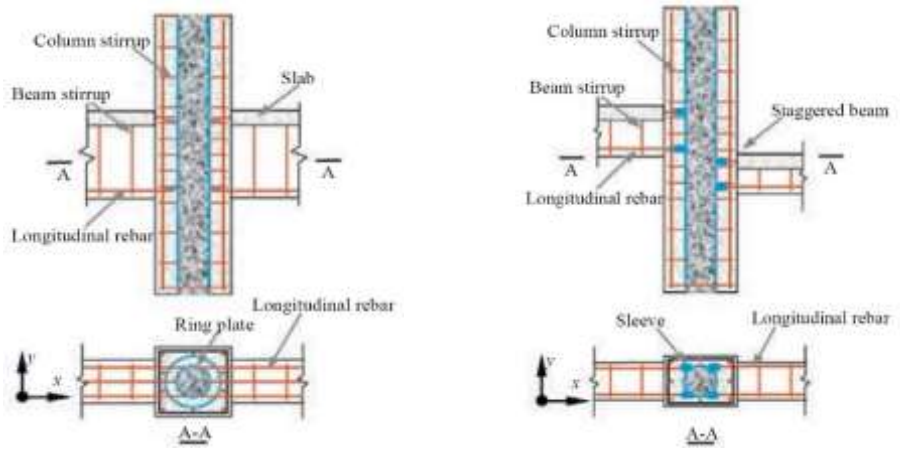

(a) (b)

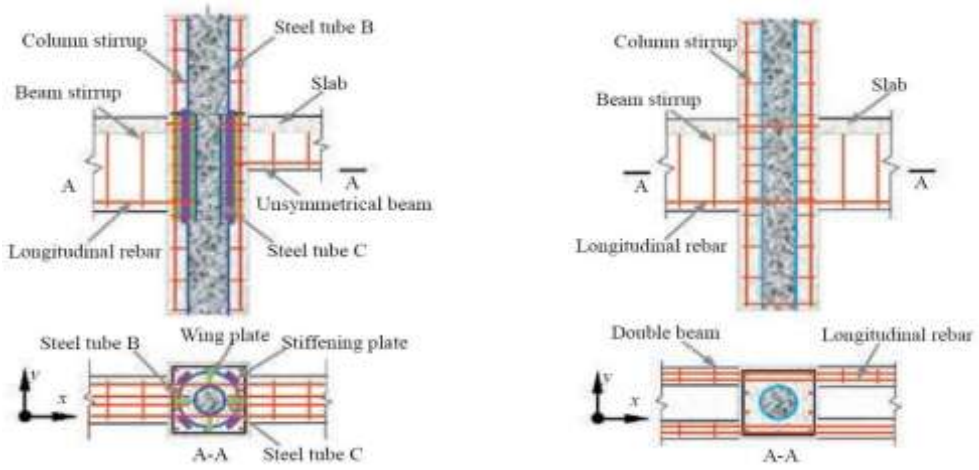

(c) (d)

Figure 2.1 Configuration of joint specimens: (a) Ring plate connection, (b) Sleeve connection, (c) Wing plate connection, (d) Anchorage connection [4]

Xu, et al., (2018) have considered the economic feasibility as well while studying experimentally the efficiency of earthquake-damaged columns reinforced by enveloped steel and reinforced seismic damage at various levels. In their work, researchers aimed at assessing the seismic efficiency of encased steel jacket-strengthened steel-reinforced concrete columns as shown in Figure 2.2. Thus, four specimens with a scale ratio of 1:2 were cast where one was an original specimen while the other was enhanced by a steel jacket. However, the other two remaining columns were pre-damaged to different degrees to simulate the moderate and severe seismic movements, and then strengthened by a steel jacket. The concrete test specimens had a rectangular cross-section of 200 mm by 270 mm with a cover thickness being held at 25 mm. Besides, the composite steel-concrete frame columns were short. Four rebars with a diameter of 16 mm were installed in each sample boundary zone. The samples' cross-section reinforcing ratio (ρ_l) was 1.60% and the stirrup ratio (ρ_v) was 0.68%. The steel ratio (ρ_a) of the specimens was 4.84%. Also, to assure the same quality of concrete, C40 type of concrete class was used from the same production run, with a curing period of 28 days. Then, three subsequent steps were accomplished. Firstly, loading the test specimens to a simulated seismic pre-damage level; secondly, reinforcement of a component with seismic damage, and finally a post-improvement low-cycle repeat load test [5].

According to the test findings, several factors that represented the seismic performance of these composite joints were evaluated. Such factors were damage model, force-displacement relation, strength and stiffness degradation, and strain response of the test specimens. Eventually, it was found that the sequence of the damage stages of the four specimens was nearly identical. Yet, there were more cracks in the steel-reinforced concrete comparative column (without damage and reinforcement). At the same time, a shear bending failure took place in the steel-reinforced concrete relative plate. Furthermore, the cracks of the encased steel jacket that strengthened the steel-reinforced concrete columns continued to increase as the amount of seismic damage increased. This, in turn, demonstrated that the encased steel jacket-strengthened specimens suppressed lateral concrete bursting at the column foot, and could not inherently prevent an increase in concrete cracks. To conclude, the impact of different axial compression ratios (23.0%, 12.9%, and 7.4%) and different reinforcement heights (500 mm, 750 mm, 1000 mm) on the seismic efficiency of steel-reinforced concrete columns with seismic damage was investigated, and the outcomes are consistent with the actual engineering requirement. The impact of different axial compression ratios and different reinforcement heights were archived based on the verification of the numerical model [5].

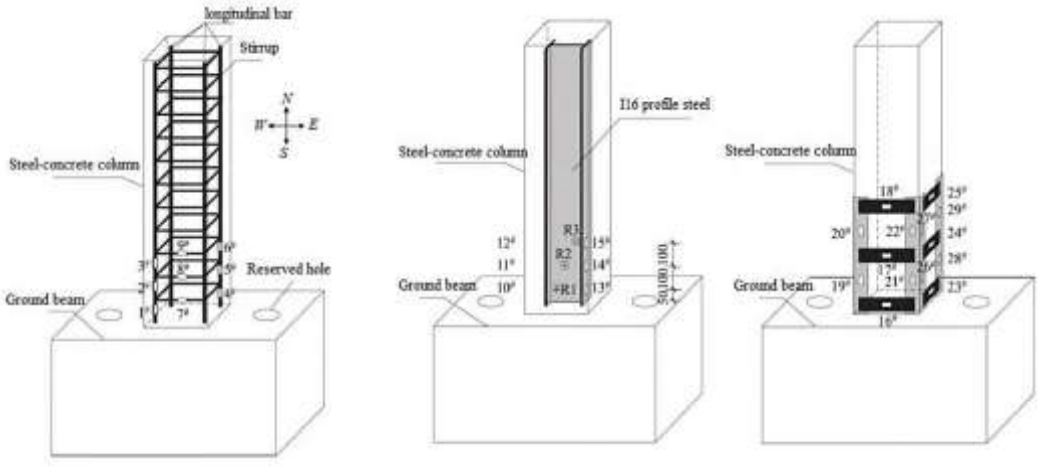

(a) (b) (c)

Figure 2.2 Column specimens: (a) longitudinal reinforcement and stirrups, (b) profile steel, (c) steel envelopes [5]

In 2016, G. Li et al. conducted both a test and parametric study of post-fire seismic performance of SRC column–RC beam joints. Besides, a numerical simulation was undertaken for studying the effect of bearing capacity and stiffness under cyclic loading. The purpose of this study was to examine the impact of some parameters like axial compression ratio, heating time, concrete strength, and profiled steel ratio on the hysteretic response of the connection after the fire. For this purpose, three specimens A, B, and C were prepared. The configuration layout dimensions for the column and beam were 1960 × 300 × 300 mm and 2870 × 300 × 300 mm respectively. This design was based on the regulations corresponding to Chinese codes (JGJ. 1996, JGJ. 2001, YB. 2007). The H-shaped steel section of the column HW175 × 175 × 7 × 10 was made of Grade Q345. Two types of bars were used for the structural elements, columns, and beams; longitudinal reinforcement bars with a diameter of 18 mm and transverse reinforcement bars with a diameter of 10 mm. The yield strength of the bars was 345 MPa and the specimens were made of concrete of a grade C40. In the analysis, however, two forms of tests were performed: the fire test and pseudo-static test. Specimen A was considered as the control one, and without direct fire effect and it was then put under the pseudo-static test. Conversely, specimens B and C were exposed to fire before the pseudo-static test [6].

The researchers in this study stated that the results obtained from the testing and the numerical simulation revealed that the stiffness and bearing capacity would be negatively affected after the fire and the longer the heating time the greater the deterioration. Besides, the increment in concrete strength, axial compression, and profiled steel ratio of the column would significantly result in improving the bearing capacity and rigidity of the SRC column – RC beam joints, except for the axial compression ratio, which had a negligible effect on the bearing capacity [6].

Kong et al. (2013) have implemented a nonlinear numerical analysis for the stress performance of an RC beam-SRC column and SRC beam-SRC column frame end joints. This analysis was done numerically by utilizing finite element software called ABAQUS. The idea behind this analysis was to investigate and compare the effect of the structural steel on the frame to that of experimental results. The developed model adopted reinforced concrete-encased steel joints with concrete compressive strength

of 30 MPa, and a welded steel I-section. In this analysis, the diameter of the longitudinal column and the beam rebars was 18 mm and the stirrup diameter was 10 mm at 100 mm in the joint and ends with 10 mm at 150 mm. The cross-sectional areas of beam and column were 200 mm by 250 mm, and 300 mm by 400 mm, respectively [7].

The nonlinear numerical modeling was performed for the stress efficiency under monotonic and cyclic loading. It was concluded that the attained results from this numerical analysis, which were obtained from ABAQUS program, had high credibility. Yet, the numerical analysis employed by ABAQUS was used to simulate component stress and deformation throughout the scope of establishing sensible boundary conditions and material constitutive relationships. Moreover, and regardless of the type of end joint, either RC beam - SRC column or SRC beam -SRC column frame connection, increasing the steel bone content, enhanced the ultimate bearing strength, and the seismic efficiency. Furthermore, in comparison to the RC beam - SRC column frame joint, the SRC beam - SRC column frame joint had greater bearing strength for structure and better seismic performance [7].

In 2010, Jacobs and Hajjar conducted a research work on load transfer in composite structural elements. The main intention of the work was to set a summary of the implementation of the load transfer-related matters. Their study comprises applying the external force to a composite structural element, distributing the force to different parts of the composite element, assessing the internal longitudinal shears that deemed necessary to be transmitted to attain this allocation of force and the mechanisms for this shear transfer in the scope of the composite member design. Besides, the researchers aimed at discussing the potential of this work concerning the transfer of composite column force. For that purpose, the approach pursued was achieved through reviewing the new AISC provisions regarding the aforementioned issues, discussing their implementation, and adding a brief technical background to the current proposed headed stud anchor, known as shear studs, regulations as they contribute to that of the transfer of load. Then, the researchers presented these additional provisions and summarized their use in the design of composite filled tubes and encased columns. To that end, the principle of the incorporation of external load

into concrete, steel or both materials contemporaneously and the determination of the longitudinal shear force needed for the equilibrium of the composite cross-section in each of these cases were investigated. Also, three potential force transferring mechanisms were addressed with a particular focus on the context of the new regulations for the headed stud anchor. Eventually, the concept of the length of the load introduction was outlined in detail [8].

In the early 2000s, Hajjar performed research work on composite steel and concrete structural systems. In this research, the aim was to summarize the previous studies on a variety of composite lateral resistance structures. These structures typically involved unbraced moment frames comprised of steel girders with concrete-filled steel tube, CFT or SRC columns; braced moment frames with concrete-filled steel tubes, and a range of hybrid and composite wall systems. The author stated that there would be a demand for the upcoming years to take into account a wide variety of new design guidelines for these composite systems, and thus providing practitioners with a rapidly expanding array of structural systems from which to assign [9].

To conclude, through reviewing past and recent studies that have been conducted on the behavior of composite column-reinforced concrete beam joints, it has become evident that the experimental and numerical investigations presented were carried out on the seismic performance of reinforced concrete-encased steel (SRC) column and reinforced concrete (RC) beam connecting joint for concentric, eccentric and biaxial loading conditions. In fact, it has been observed that studies on (SRC) column (RC) beam connection using various percentages of structural steel are limited. For instance, the behavior of these composite joints with different ductility design considerations has not been fully addressed. Moreover, the effects of several parameters, like structural steel ratio and tie spacing on the strength and ductility of such type of composite connections, need to be analyzed. As mentioned previously the Turkish Standard, TS 500, and Turkish Earthquake Code, TEC 18, do not include any capacity prediction equations on composite elements. Therefore, in this study, the verification of the ductility of (SRC) column (RC) beam joint will be quantified at the same level as the strength as well as stiffness, and a then set of recommendations will be addressed concerning the codes.

CHAPTER 3

EXPERIMENTAL WORKS

This chapter mainly addresses the details of an experimental study to investigate the seismic performance of the SRC column with headed shear studs and RC beam joints. This work is conducted at the Atilim University's Structural Mechanics Laboratory, Ankara. Essentially, the effort is directed towards understanding the composite beam-column joint seismic efficiency and vulnerability to shear and axial failures. Therefore, the reinforcing steel ratios of the structural elements included in the testing approach are deemed the key variables. Besides, the axial loads are applied concentrically on top of the columns while the lateral load is applied on both sides of the frame specifically at the region of intersection between the beam and the column. As mentioned earlier in this study, it is aimed at identifying the comprehensive seismic efficiency of the proposed joints, investigating the joint shear strength in different joint configurations, and evaluating the effect of axial load on the performance of the proposed joints. The outcomes of this work might also serve as a reference for calibrating and evaluating joint shear strength and axial efficiency models (future works). An overview of the test specimens, test setup, and loading conditions are discussed throughout the following sections.

3.1. Test Parameters

For the sake of this work, the necessary test parameters are specified based on prior studies of joint experiments with targeting the assessment of problems related to the strength and deformation capacity that have been undetermined yet. In the tests, the key parameter is the variation of the transverse steel reinforcement ratio in the structural members in the columns in particular. Test specimens are designed as high and low ductile to examine the seismic behavior and strength of structural members subjected to concentric axial and lateral reversal cyclic loads. The vertical structural members are fabricated with different percentages of transverse steel reinforcement to

monitor the variation in the ultimate load-carrying capacity of the columns and capability of the composite joint to withstand lateral loads. In both frames, the structural steel in the columns is oriented and tested about the strong axis bending.

3.1.1 Column transverse reinforcement ratio

The transverse reinforcement ratio has a very great effect on the seismic performance of the joint. It has been stated that increasing the ratio of the transverse reinforcement resulted in more ductile behavior [10]. Two ratios are adopted for HD and LD columns, 1.93% and 1.45%, respectively. The ratio of transverse reinforcement, shown in equation (3.1), is defined as the total cross-sectional area of the stirrups divided by the cross-sectional area of the column. It is noteworthy to mention that both frames were designed according to the Turkish Earthquake Code (TEC 18).

$$\rho = \frac{n\,As}{Ag} \tag{3.1}$$

Where ρ is the transverse reinforcement ratio, n is the number of stirrups, A_s is the cross-sectional area of transverse reinforcement, A_g is the gross cross-sectional area of the column.

The other test parameters which are considered here are the joint aspect ratio, the cyclic lateral load ratio, and the axial load ratio as demonstrated below in Table 3.1. These parameters are defined in the following parts:

Table 3.1 Test parameters

Specimen ID	Joint Aspect Ratio, α	Column Transverse Reinforcement Ratio	Axial Load (kN)	Cyclic lateral load (kN)
HD	1.2	1.93%	150	300
LD	1.2	1.45%	150	300

Note: HD refers to the high ductile frame, where LD refers to the low ductile frame.

3.1.2 Joint aspect ratio

The joint aspect ratio has been proven to be one of the most important factors affecting a joint's efficiency. The most commonly used definition of joint aspect ratio, which assumes the whole joint as a shear panel that transfers loads by direct normal and shear stress, is the ratio between beam depth (h_b) to column depth (h_c); that is,

$$\alpha = h_b/h_c \tag{3.2}$$

The increment in the joints aspect ratio will increase in the resisting moment of the joint and hence increases its moment capacity. However, the value of this ratio is designated to be 1.2 to underline the practical upper and lower bounds for both specimens. Based on theoretical and experimental observations of joint tests, the impact of this ratio on the joint shear strength is well defined. In line with this, Vollum and Newman [11], Bakir and Boduroglu [12] have proposed a directly correlated linear relationship between the joint shear strength and the joint aspect ratio ranging between 1 and 2.

3.1.3 Lateral reversal cyclic load

The specimens were tested against reversal cyclic loading according to ACI 374.1-05 [13] and the cycles were attributed to predetermined drift ratios as specified in the following points.

1. Three fully reversed cycles must be applied at each drift ratio.
2. The initial drift ratio shall be within the essentially linear elastic response range for the module. Subsequent drift ratios shall be to values not less than one and one-quarter times, and not more than one and one-half times, the previous drift ratio.

Based on the aforementioned points, the actuator was first pushed and pulled to drift ratio of 0.2% (displacement of ±3 mm), then the drift ratio was gradually increased by one-quarter times the previous drift ratio that is 0.2%, 0.25%, 0.35% till it reached the ratio of 1.75%. The actuator used in this test has a maximum capacity of 300 kN and a stroke length of 500 mm. The tests were conducted by applying cyclic loading using

a displacement-control approach. It is important to mention that the 1.75% drift level is the maximum achievable drift level due to the limited laboratory capability.

3.1.4 Axial load

For the effect of the axial load on the shear strength of joints, some researchers have claimed that the shear strength of joints improves with the increment of axial load [13, 14]. Nonetheless, it has been reported in other studies that the shear strength of a joint is not influenced by the axial load rate [15, 16, 17] and further study [19] suggests that shear strength drops with the increase of axial load. Determining the effect of the axial load on the shear strength of joints is not simple because of the complex mechanisms associated with joint response to the shear. The great majority of researches on this issue concludes that higher axial load lessens ductility and leads to fast degradation of strength after failure initiation. The real impact of the axial load is noticeable when greater than 0.2 $f_c'A_g$ axial load is applied. Around the limit of 0 to 0.2 $f_c'A_g$, the change in joint shear strength due to the increase of the axial loading is not as dramatic as the impact of raised axial load above 0.2 $f_c'A_g$. Moreover, it is conceivable that higher axial load raises the strength of the bond of the beam bars held in the joint, which in turn improves the flexural strength of the beam and thereby the joint strength [14].

Since the main objective of this study is to investigate the seismic performance and the effect of axial load on the joint shear strength and deformability, it was decided to choose a gravity axial load ratio of 0.1 to represent a considerable percentage of the minimum load that might be applied on the columns. Therefore, it was decided to (3.3), the compressive strength of the composite column was calculated according to TS 500 considering both the concrete and the structural steel.

$$P_n = N_{dm1} + N_{dm2} \tag{3.3}$$

Here, P_n is the axial compressive strength of the composite column, N_{dm1} is the axial compressive strength of concrete ($N_{dm1} \leq 0.4 f_{ck} A_c$), N_{dm2} is the axial compressive strength of the structural steel ($N_{dm2} \leq \sigma_y A_{st}$), f_{ck} is the characteristic compressive

strength of concrete, A_c is the cross-sectional area of concrete, σ_y is the yield strength of structural steel, A_{st} is the cross-sectional area of structural steel.

3.2. Test Program

The half-scale SRC column to the RC beam joint was designed with some adjustments to accommodate laboratory space. The specimens were designed to exhibit the real seismic performance and efficiency of the composite joints when exposed to cyclic lateral loading as well as axially applied loads on the columns. The overall geometry with a 3D viewing of the test specimens was demonstrated in Figures 3.1 and 3.2. Additionally, all of the structural members were designed according to the current TS500. The sectional analysis performed by hand calculations and verified utilizing SAP2000.

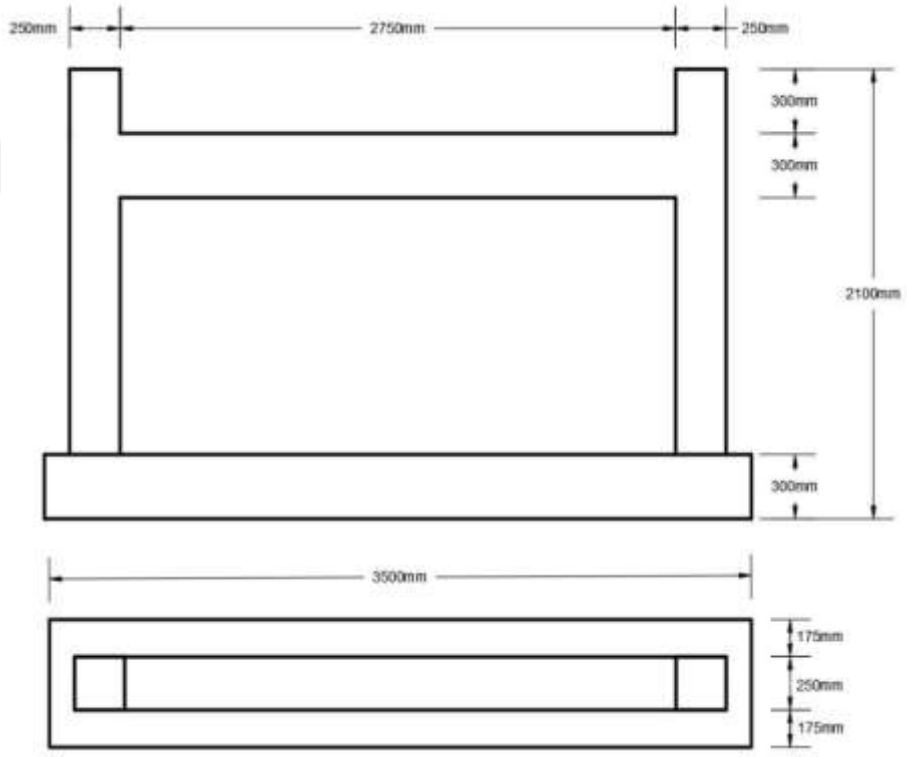

Figure 3.1 The overall geometry of test specimens

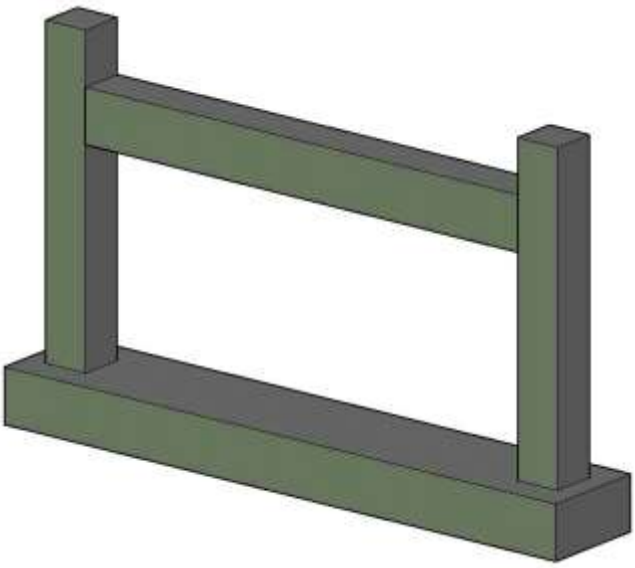

Figure 3.2 The overall 3-dimensional view of the test specimen

3.2.1 Description of test specimens

Two frames, each consisting of square SRC columns with headed shear studs to RC beam, were tested for concentrically applied axial loads and lateral reversal cyclic load. These frames were constructed with different transverse reinforcing steel ratios in the columns with the same percentages of I-shaped structural steel and concrete strength.

The first specimen was constructed to be as high ductile (HD), the second one was constructed as low ductile (LD); however, normal strength concrete was used for both specimens. The cross-sectional area of the columns was 250 mm × 250 mm and the effective length of these columns was fixed at 1500 mm with a slight upward extension of 300 mm. The columns were tested for the concentric axial load. The diameters of the main transverse and longitudinal reinforcements in these columns were 8 mm and 10 mm, respectively. The column with the low ductile design was constructed with a stirrup spacing of 70 mm at the confinement zone (250 mm length) and 120 mm at the mid-zone (700 mm length), while the other column with the high ductile design was with a spacing of 50 mm at the confinement zone (250 mm length) and 120 mm at the mid-zone (700 mm length). Figure 3.3 illustrates the transverse and longitudinal reinforcements in the columns.

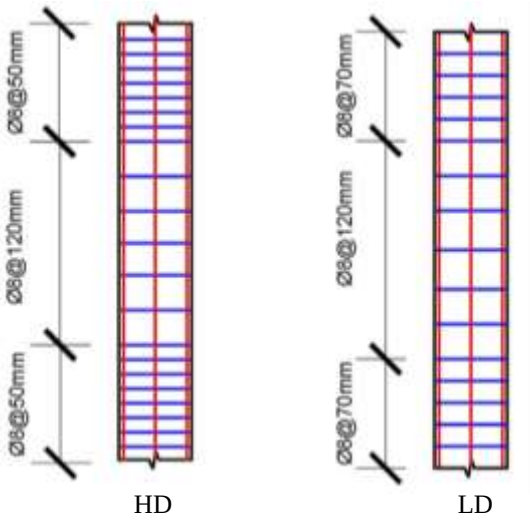

Figure 3.3 Reinforcement detailing in the columns

The compressive strength of the concrete (f_{cu}) for the columns which is 30 MPa was identical with that for the frames. The yield strength of reinforcing steel and the structural steel is 428 MPa and 317 MPa, respectively. The I-shaped HEB100 cross-section for the structural steel sections shown in Figure 3.4 was selected considering all the limitations of available codes for composite columns.

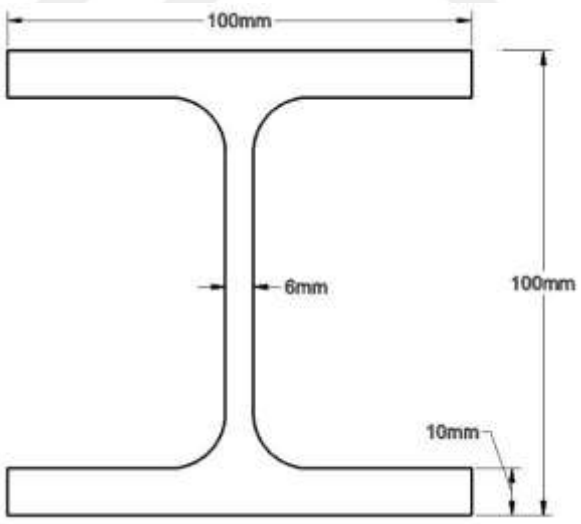

Figure 3.4 HEB100 structural steel section

The transverse structural members; on the other hand, had a cross-sectional area of 250 mm × 300 mm with main transverse and longitudinal reinforcement diameters of 8 mm and 12 mm, respectively. Both transverse structural members of the frames have the design with a stirrup spacing of 75 mm at the confinement zone (575 mm length) and 140 mm at the mid-zone (1600 mm length). The concrete average compressive strength (f_{cu}) for the transverse structural members is 30 MPa. The yield strength of reinforcement is 428 MPa. Figure 3.5 depicts the reinforcement details in the beam.

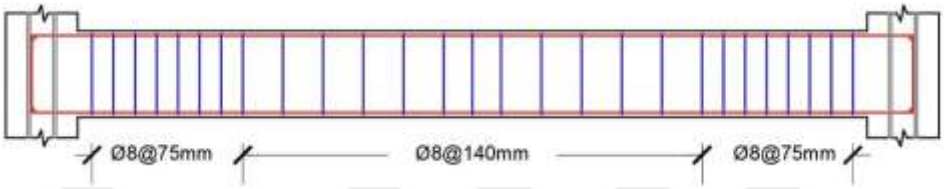

Figure 3.5 The reinforcement details in the beam

The foundation was a combined footing and was designed to support two columns of the same load applied (symmetrical) on both. For both frames, the foundation was identical and its cross-sectional area was 300 mm × 600 mm with a length of 3,500 mm as shown in Figure 3.6. While testing, these foundations were placed and fixed on two I-shaped steel sections. Besides, in these foundations, the diameters of the main transverse and longitudinal reinforcements were 10 mm and 12 mm respectively as depicted in Figure 3.7.

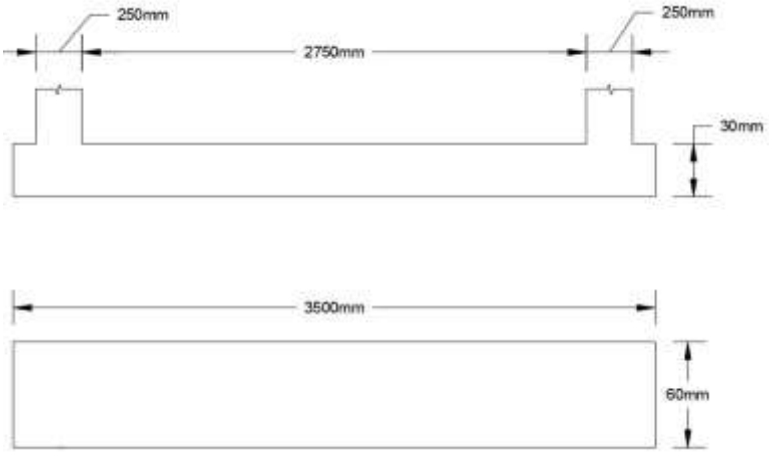

Figure 3.6 The geometric parameters of the foundation

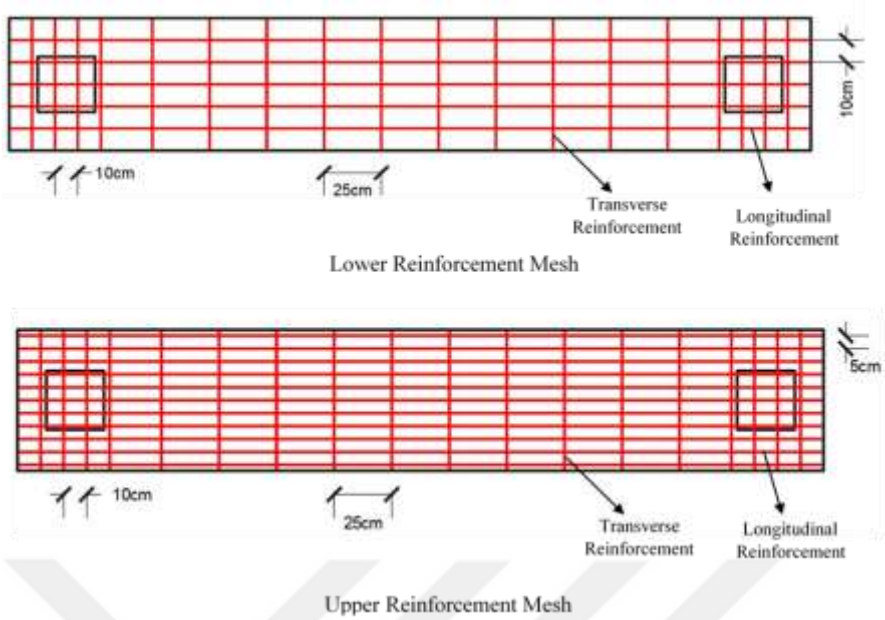

Figure 3.7 The reinforcement detailing of the foundation

The geometric properties and the reinforcement detailing of the test specimens for high and low ductile frames are given in Tables 3.2 and Figure 3.8, respectively.

Table 3. 2 Test matrix and specimen geometric properties

ID		HD					LD				
Beam	Size (mm)	Reinforcement				Size (mm)	Reinforcement				
		Long.		Transverse			Long.		Transverse		
		Top	Bottom	Confine. Zone	Mid-Zone		Top	Bottom	Confine. Zone	Mid-Zone	
	250×300	4Ø12	4Ø12	Ø8@75mm	Ø8@140mm	250×300	4Ø12	4Ø12	Ø8@75mm	Ø8@140mm	
Column	Size (mm)	Reinforcement				Size (mm)	Reinforcement				
		Long.	Transverse				Long	Transverse			
			Confine. Zone		Mid-Zone			Confine. Zone		Mid-Zone	
	250×250	8Ø10	Ø8@50mm		Ø8@120mm	250×250	8Ø10	Ø8@70mm		Ø8@120mm	
Foundation	Size (mm)	Reinforcement				Size (mm)	Reinforcement				
		Long.		Transverse			Long.		Transverse		
		Upper	Lower	Upper	Lower		Upper	Lower	Upper	Lower	
	300×600	Ø12	Ø12	Ø10	Ø10	300×600	Ø12	Ø12	Ø10	Ø10	

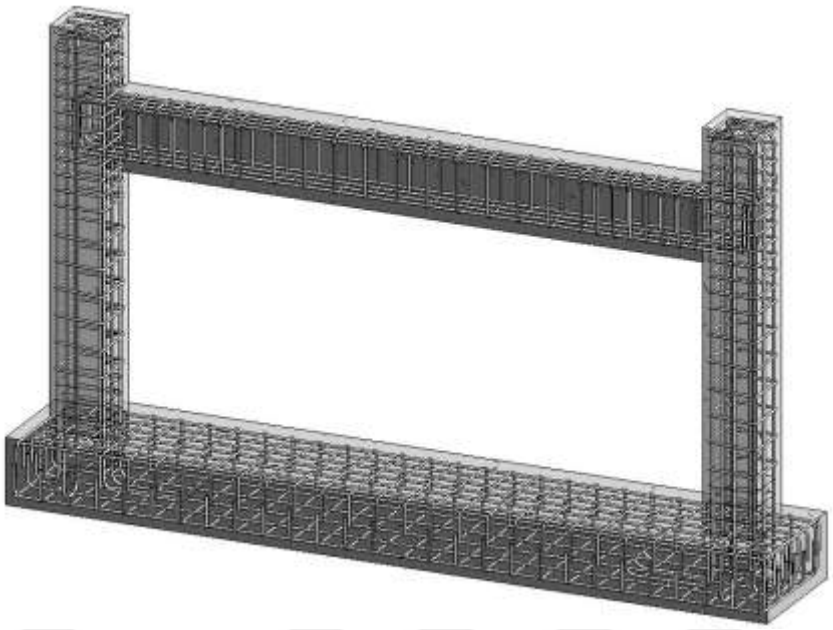

(a)

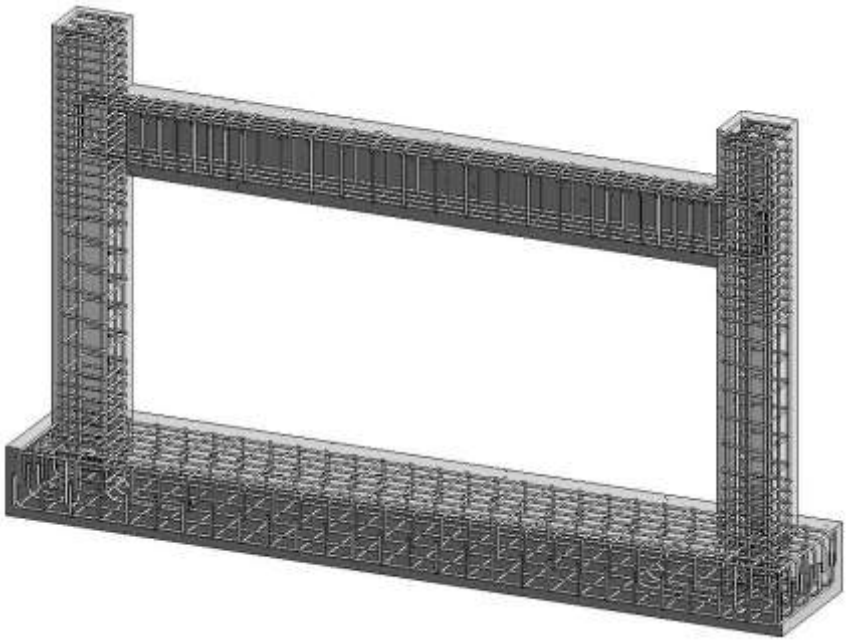

(b)

Figure 3. 8 The dimensional reinforcement detailing of the test specimens:
(a) Low Ductile, (b) High Ductile

3.2.2 Structural elements fabrication

3.2.2.1 Column fabrication

The SRC columns mainly comprise two parts namely the steel cage and the concrete as shown in Figure 3.9. The steel cage consists of I-shaped structural steel, longitudinal reinforcements, and transverse reinforcements. The structural steel sections were provided by a local firm in Ankara. As a final step, concrete was placed in the steel cage for the construction of the frames.

The steel cage consisting of steel I-section and longitudinal and transverse reinforcements are constructed in the Structural Engineering Laboratory of Atilim University, Ankara, Turkey.

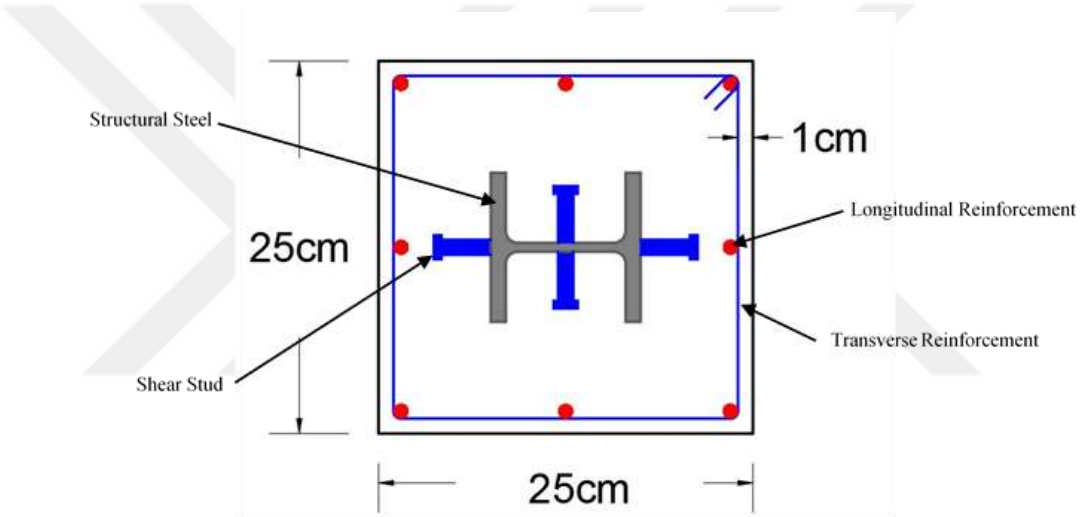

Figure 3.9 SRC column cross-section

3.2.2.1.1 Steel section fabrication

The I-shaped structural steel sections (HEB100) as shown in Figure 3.10 were constructed according to the design drawings. This section was chosen among the other wide flange sections because it is the most used one in practice.

Figure 3.10 HEB100 structural steel section with shear studs

3.2.2.1.2 Shear studs fabrication

Shear studs normally act as embedment anchors on miscellaneous embedded plates like structural steel members; therefore, they were welded to the metal component. Shear studs used in this project are as demonstrated in Figure 3.11. These studs were designed in line with AISC [20] Specification for composite columns as composite shear transfer components, and were welded at every 200 mm along the steel section on all sides; that is, on both webs and flanges.

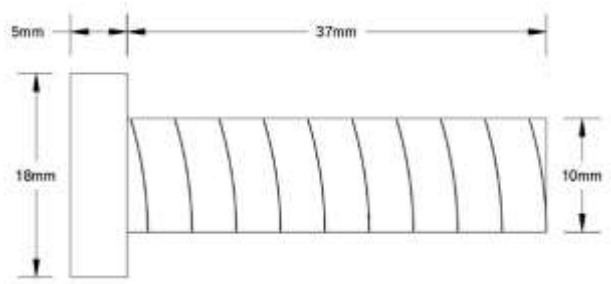

Figure 3.11 Shear stud dimensions

3.2.2.1.3 Steel reinforcement

Two different diameters of reinforcements (that is, main reinforcement and hoops) were implemented for the erection of the composite columns. The size and arrangements of the rebars are described in detail in Section 3.4.1. The transverse and longitudinal reinforcements were both bent and shaped according to the specifications mentioned in the Turkish Earthquake Code 2018 [21].

3.2.2.2 Beam fabrication

RC beams consist of reinforcing steel and concrete as shown previously in Figure 3.5. Reinforcing steel involves longitudinal and transverse reinforcements. The longitudinal and transverse reinforcing steel were cut, shaped, and constructed in the laboratory. Finally, concrete was placed after the formworks had been constructed.

3.2.2.3 Foundation fabrication

The combined footing used was made up of main and transverse reinforcing steel and concrete as shown previously in Figure 3.7. The steel mainly involves upper and lower reinforcement meshes. As for the previous structural elements, the reinforcing steel was cut, shaped, and constructed in the laboratory. Lastly, concrete was placed after the formworks had been constructed.

3.2.3 Specimens construction

The site of construction was at the Structural Engineering Laboratory of Atilim University. At first, the steel reinforcement was cut, prepared, and formed according to the structural drawings. The following step was constructing the wooden frameworks for the specimens. Throughout the construction of the forms, great concern was given to leveling these wooden forms to mitigate the potential impact of any eccentricities that might be induced due to the complexity of the configuration of the test specimens. Likewise, the wooden forms of the beams were extensively supported after construction to avoid any tilt or failure during and after concrete casting. The sides of the column forms were also adequately stiffened before casting to avoid lateral bulging. Furthermore, these forms contain holes at certain positions to fit the bars at both columns and both ends of beam forms that were used to hold the LVDTs to measure relative displacement changes between those bars.

The phase of placing steel reinforcement has begun with fixing both the column longitudinal reinforcement and transverse hoops and then inserting the

structural steel into the column cage. The next phase included the fabrication of the lower steel meshes of the foundation followed by fixing the columns on the lower mesh of the foundation and then the upper steel mesh was fabricated. Lastly, the fabrication of beam reinforcement took place as indicated in Figure 3.12. It is important to mention that the installation of the hooked beam longitudinal reinforcement in the joint was a highly demanding task since the structural steel section was too tiny to bend the beam bars inside (Figure 3.13). The sequence of fixing reinforcing bars of the beam at the joints was as follows: placing the beam bottom inner longitudinal reinforcement first and then the beam top inner longitudinal reinforcement; placing the bottom outer beam longitudinal reinforcement and then the top outer beam longitudinal reinforcement.

(a) (b)

(c)

Figure 3.12 Specimen construction stages: (a) Steel cage construction of the columns. (b) Steel reinforcement meshes of foundation. (c) Steel reinforcement construction of the beam

Figure 3.13 Congested beam steel hooks inside the joint

After completing the reinforcing steel installation, the steel reinforcement was undergoing a strain gauging process at multiple venues (positions). A detailed labeling technique has been applied to the gauges mounted on the steel reinforcement, which in turn enables identifying those locations (positions) by rapid inspection of the label. The strain gauges were installed in their estimated positions, giving serious attention to installation accuracy to guarantee that the positions of the strain gauges suited the

intended design. The strain gauge cables were prolonged, tapped, and directed outside until the allocated exit point (at low-stress locations) was reached in the framework. Prior to concrete casting, final verification on framework dimensions, reinforcing steel alignment, and orientation and the concrete cover were completed. Likewise, the inner surface of the wooden framework was witted.

To facilitate concrete casting in the congested zones of specimens; in particular, the headed bar regions and joint hooked bar intersections, the mix design proportions required 80 mm of a slump. The casting phase was essentially divided into two stages, beginning with the combined footing in the first stage and followed by casting the beams and the column in the second stage (Figure 3.14). The concrete was compacted to a great extent with electrical rod type vibrators, which were applied internally to the fresh concrete poured in the framework and externally to the column surfaces as depicted in Figure 3.15. After casting, a trowel was used to flatten the surface of the concrete. Since the cast samples were placed indoors in a very typical environment, there was no need for special care that could impact the strength of the concrete.

(a)

(b)

Figure 3.14 Concrete casting stages: (a) Concrete casting of foundation. (b) Concrete casting of beam and columns

Correspondingly, the chosen approach of curing involved leaving the cast specimens within wooden frameworks for three days and watering the exterior surfaces of the specimens regularly using freshwater potable water. Test specimens' parts were in two different casting days; on the first day, the foundations were cast, a month later the other structural elements of the specimens (columns and beams). The finished specimens are shown in Figure 3.15.

Figure 3. 15 Test Specimen

An overall number of 12 standard concrete cylinders of 150 mm diameter and 300 mm height have been tested. They were sampled from fresh concrete to describe the properties of each cast specimen (Figures 3.16). Thus, these concrete cylinders were put in compression testing to observe the average compressive strength of concrete at a certain period until the test date. At the test date, three concrete cylinders were tested for the same property; that is, the compressive strength. However, concrete cylinders were kept in pools of water.

Figure 3.16 Standard concrete cylinders

3.2.4 Concrete mix for the frame

The principal property considered during the mix design was the compressive strength such that the whole batches were verified for this intended property. For casting the parts of the frames, a normal-strength concrete of 30 MPa was used. This normal-strength concrete was used for casting two composite frames; i.e. two columns (250 mm × 250 mm × 1500 mm) and one beam (250 mm × 300 mm × 3000 mm) as well as the 12 standard concrete cylinders. Besides, 20 mm downgrade crushed stone and the sand of 4 mm were used as a coarse aggregate and fine aggregate, respectively. The cement type used in the concrete mix was Portland cement. The mix design for one cubic meter is presented in Table 3.3.

Table 3.3 Mix proportion design

C30 MIX ($1m^3$)		
Material	**Quantity**	
Fine aggregate	746	kg
Coarse aggregate	992	kg
Cement content	417	kg
Water content	200	kg
Total Amount	2355	kg/m^3

3.2.5 Material properties

The columns are composed of I-shaped structural steel, longitudinal and transverse reinforcement, and concrete whereas the beams and foundations are composed of only longitudinal and transverse reinforcement and concrete. To determine the strength of the steel sections and reinforcing steel, a tensile test was performed on samples of steel plates and rebars. In contrast, concrete cylinders were cast and tested to determine the compressive strength.

3.2.5.1 Structural steel

As indicated earlier in this chapter, the I-shaped steel columns were as HEB100 sections. The structural steel ordered from the factory with a defined average yield strength of 317 MPa.

3.2.5.2 Steel reinforcement

The steel reinforcements used for constructing the composite frames are Ø10 mm and Ø12 mm for the main reinforcement and Ø8 mm for stirrups. The main reinforcement of Ø10 mm was used as longitudinal reinforcement for columns and reinforcement of Ø12 mm was used as longitudinal reinforcement for beams. The stirrups of Ø8 mm were employed along the length of the columns and beams. The tensile testing for rebars was conducted and the average yield strength was estimated as 428 MPa.

3.2.5.3 Concrete

It was required to batch four mixes of concrete for the two frames. The cast concrete used for constructing these frames was C30. However, to determine the properties of concrete; in particular, the compressive strength, a total of twelve concrete cylinders with 150 mm diameter and 300 mm height were cast as illustrated in Figure 3.16. For that reason, three cylinders were cast for each value of strength. After 24 hours of casting, cylinders were removed from molds and kept in water pool. Concrete cylinders were then brought out after 30 days to determine the compressive strength of concrete. The values of the compressive strength of all concrete cylinders are given in Table 3.4. It can be seen clearly from these results that there is a slight variation in strength values; this is due to the reason that concrete mixes were conducted manually.

Table 3.4 Compressive strength of cylinders specimens

Foundation of LD Frame		**Foundation of HD Frame**	
Specimen ID	f_{ck} (MPa)	Specimen ID	f_{ck} (MPa)
S1-1	21.7	S2-1	22.6
S1-2	24.0	S2-2	25.9
S1-3	26.8	S2-3	29.7
Mean	*24.2*	*Mean*	*26.1*
LD Frame		**HD Frame**	
Specimen ID	f_{ck} (MPa)	Specimen ID	f_{ck} (MPa)
S1-1	32.54	S2-1	33.1
S1-2	33.2	S2-2	28
S1-3	32.5	S2-3	32.41
Mean	*32.75*	*Mean*	*31.17*

3.3. Test Setup

The test setup is particularly designed and constructed to represent the real boundary conditions of the system as close as possible to meet the specifications of the loading procedure. The horizontal translation of beams is certainly allowed. There are multiple elements in the test setup; vertical axial loading system, lateral cyclic loading system, lateral restraint system at the foundation. The schematic diagram of the test setup is

illustrated in Figure 3.17, whereas Figure 3.18 shows the test specimen installed in the actual laboratory setup.

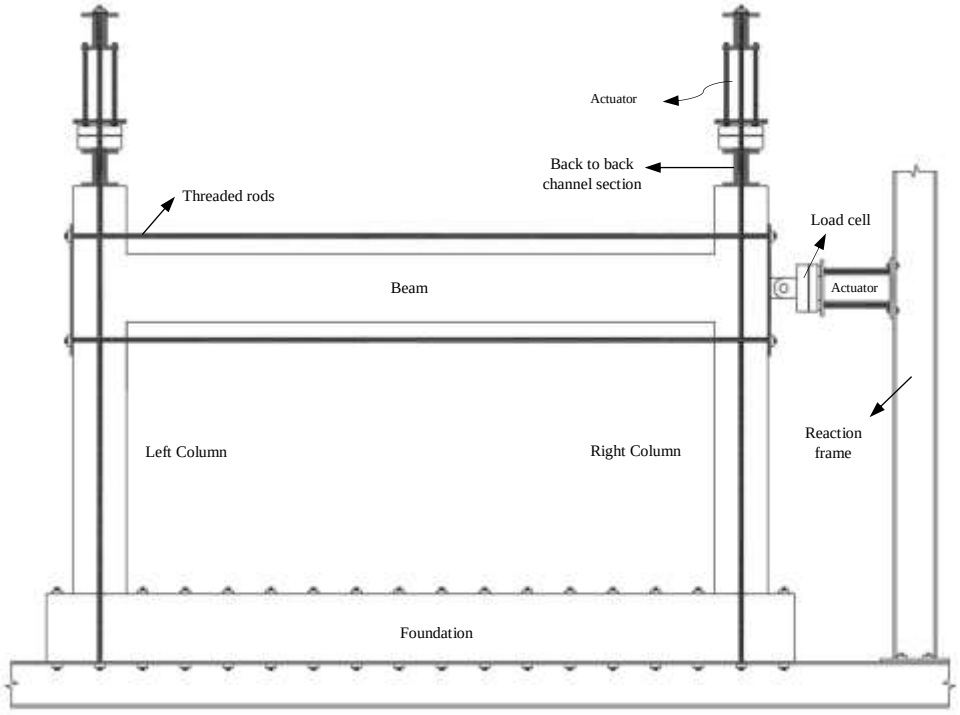

Figure 3.17 A schematic diagram for the test setup

Figure 3.18 Test specimen installed in the actual laboratory setup

The loading system presented in Figure 3.17 has a loading capacity of 300 kN fixed on a portable crosshead and applies cyclic compressive force laterally. The base of the actuator sits on a high structural steel platform. In addition, the axial load applied on the columns was achieved using threaded rods attached to the channel. Two channel sections were used; one above the column and the other below the foundation to squeeze the columns by screwing the rod.

3.4. Test Instrumentations

The test specimens were set to measure the global response, local deformations, and strains employing 40 data channels per test. The instrumentation scheme comprises internal devices namely electrical strain gages to measure steel strains and external devices (linear variable differential transformer, LVDT) to measure the relative deformations of different points on the concrete surface which can roughly refer to concrete strains. Besides, the test setup was positioned for measuring the local strains at lateral restraint system as well as measuring the overall deformation of the different elements of the setup.

3.4.1 Internal instrumentation: Steel strains gauges

Reinforcement bars were instrumented using 120±0.5 Ω resistance electrical strain gauges at the locations indicated in Figure 3.19. Each test specimen was instrumented using exactly 20 strain gages. Column bars were gauged at four locations; the column joint interface sections at two of the corner longitudinal bars of the columns where the most critical flexural sections and two strain gauges on the hoops located at the column joint interface. Only edge bars in the beam were instrumented. The beam bar gauge locations were chosen to achieve a measure of the strain profile over the regions of interest, namely the joint region and the potential plastic hinge region of the beam. The joint region of the longitudinal beam bar included four gauges as shown in the figure. Both joints in the frames were gauged identically.

Transverse reinforcement of the beams was lightly gauged (two gauges at the second stirrup from the beam-joint interface) to monitor shear and torsion strains of the beams.

Two hoops of the column transverse reinforcement that were parallel to the beam level were instrumented to obtain the tendency of those hoops to resist the lateral loads applied. Special care was given to the process of strain gauge installation to ensure full protection of these vulnerable electric devices. The reinforcement bar was smoothened over 5 cm length. Next, the smooth bar surface was chemically treated and cleaned. The strain gauges were then mounted using clear film of special adhesive agent. After installing the gauges, several protective coating layers were applied to them. That included a silicon wax layer to keep moisture out, an adhesive flexible tape layer to articulate the gauge and to ensure sufficient protection during concrete casting.

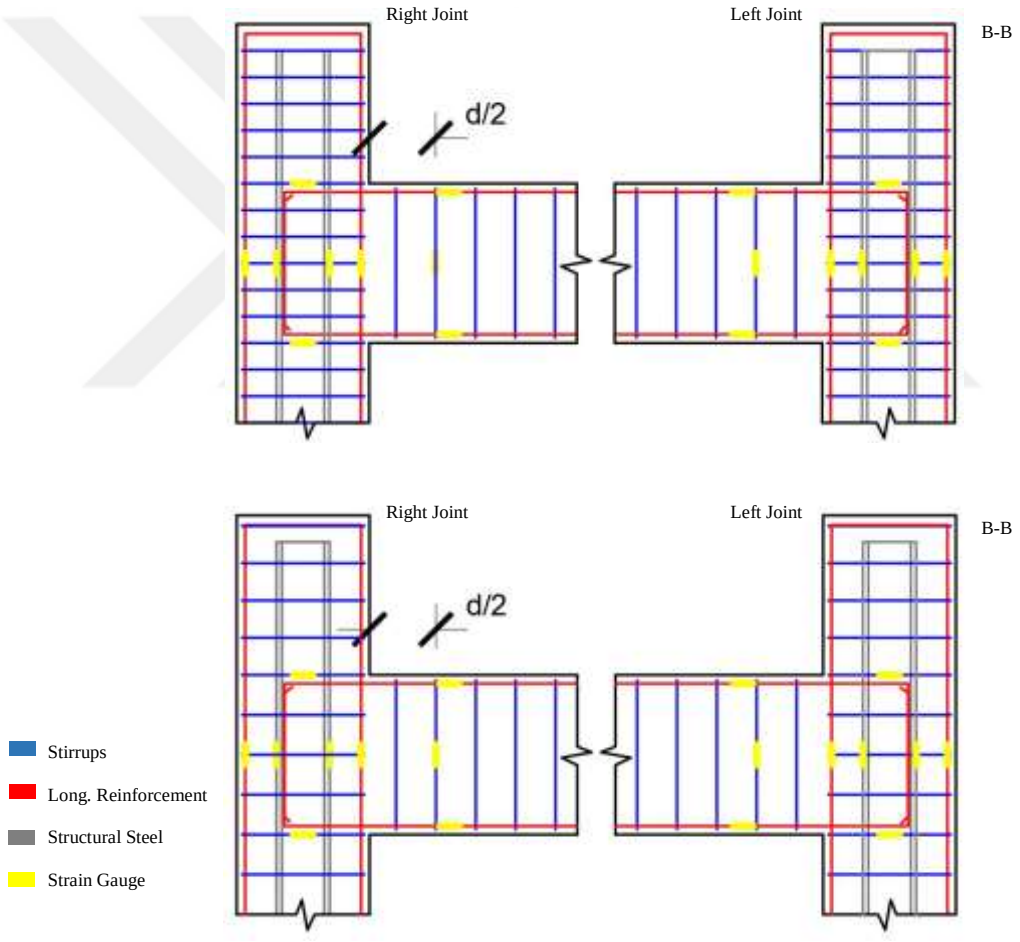

Figure 3.19 Strain gauge locations

3.4.2 External instrumentation: Linear variable differential transformer

Linear variable differential transformer (LVDT) was used to measure both global deformations and relative displacement between different points on the concrete surface of the specimen. The LVDT instrumentation scheme is depicted in Figure 3.20. The LVDTs were installed on Ø8 mm diameter stiff reinforcing steel bars that were embedded in the subassembly before concrete casting. The steel bars penetrated the entire depth (or width) of the element they are embedded in. The distances between the steel rods were chosen prior to construction according to the designed layout. The response quantities of interest were joint shear strains, joint axial and transverse strains, column axial and shear deformations, beam longitudinal deformations, beam shear deformations, relative beam-column rotation, column and beam curvatures, column and beam torsional deformations, and lateral restraint system strains.

Figure 3.20 The LVDT instrumentation scheme

CHAPTER 4

EXPERIMENTAL RESULTS AND DISCUSSION

This chapter discusses the test results of the experimental investigation carried out in this thesis. The chapter concisely presents and explains the general performance of the test models and the response of the proposed joints.

An overview of the key results of the test includes the maximum lateral load applied to reach 1.75% drift level along with the associated yield loads, and lastly attributed with the first crack loads are illustrated in Table 4.1. The drift ratio can be obtained by dividing the lateral displacement of the beam tip by the column length.

Table 4.1 Key test results of the frames

Specimen ID	Maximum load applied to reach 1.75% drift (kN)	Lateral load at first column rebar yield(kN)		Lateral load at first beam rebar yield(kN)		First crack load (kN)
		Left	Right	Left	Right	
HD	268.08	Not Yielded	Not Yielded	127.98	152.65	57.29
LD	260.99	Not Yielded	Not Yielded	155	277	78.91

The lateral loading system was conducted based on the displacement-control mechanism, in which the displacement sequence was applied gradually until the end of testing as depicted in Figure 4.1 and Table 4.2. Each load step consisted of three fully reversed cycles. This loading sequence was applied to maintain a constant increment of displacement, neither too large nor too small, till the end of the test.

In fact, the maximum drift that can be achieved in the laboratory depended on the amount of load that can be applied. The load needed to attain that deflection was predicted considering the joint capacity of the frame. For the joint capacity determination; however, the AISC-LRFD [20] specification states that the shear

capacity for the concrete-encased composite members should be computed considering the steel section properties and the shear capacity contribution of the reinforced concrete portion is ignored. Furthermore, the ACI Code [22] does not provide detailed guidance for the shear design of the concrete composite members. Therefore, it was decided to consider the ACI 318 for preliminary estimation of the capacity of the joint considering only the RC portion as considered in the ACI 318.

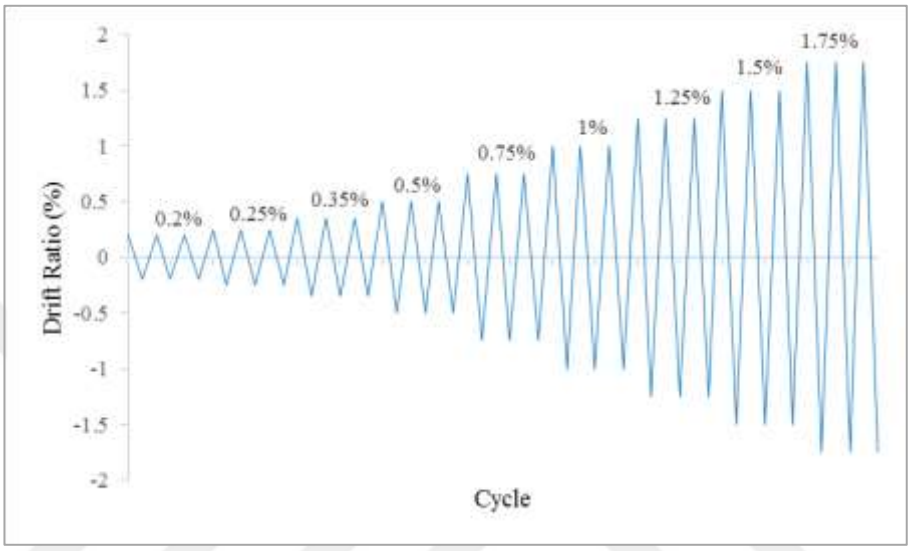

Figure 4.1 Pattern of cyclic displacement

Table 4.2 Lateral displacement sequence of the frames

Loading Step	Number of Cycles	Amplitude (mm)	Drift Ratio (%)
1	3	3	0.2
2	3	3.75	0.25
3	3	5.2	0.35
4	3	7.5	0.5
5	3	11.25	0.75
6	3	15	1
7	3	18.75	1.25
8	3	22.5	1.5
9	3	26.25	1.75

4.1. Crack Patterns

Crack patterns and shapes throughout the visual observation of each specimen failure mode attributed to the reached drift ratios during loading are depicted for the two specimens in Figure 4.2 and Figure 4.3. The numbers written next to each crack in the figure refer to the drift ratio level.

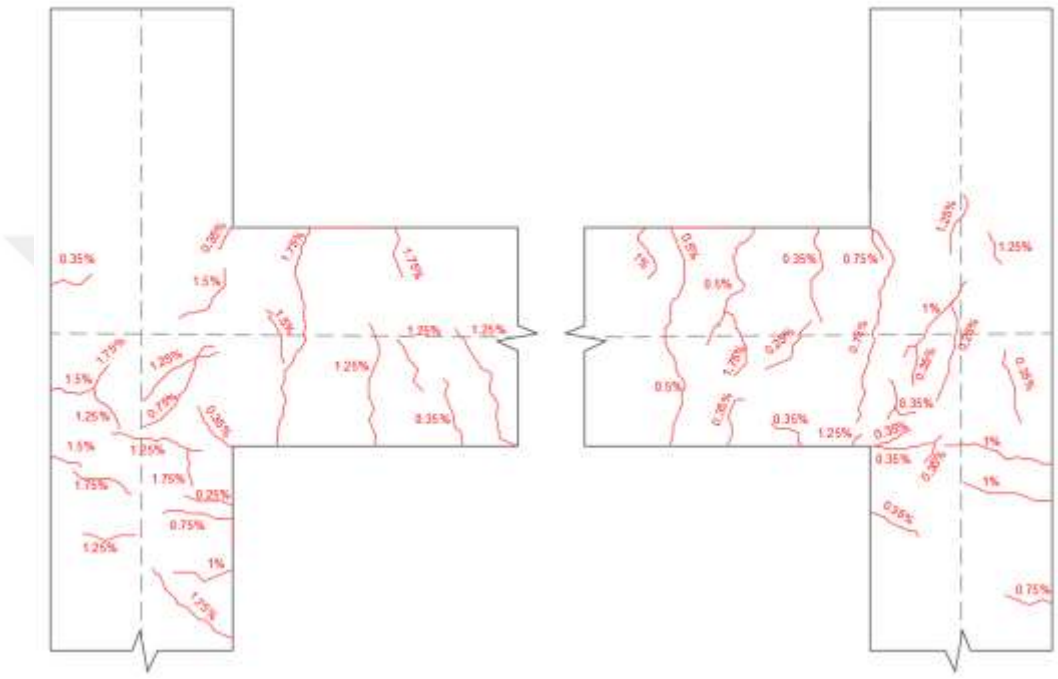

a) Left joint b) Right joint

Figure 4.2 Crack pattern of the low ductile frame attributed with drift ratio at which the crack occurred

At the left joint in Figure 4.2, the first cracks at the upper and lower beam-column angles were observed at a drift level of 0.35%. Throughout the repeated loading action, major cracks, and other small parallel cracks developed and these cracks expanded towards the centerline of the beam. The inclined shear cracks in the sample were found at drift levels of 1.25% and 1.75%, becoming more recognizable at 1.75% when reached the beam axis. For drifts around 0.75% to 1.25%, slightly inclined vertical cracks started to emerge on the core of the column. The composite joint demonstrated several other inclined cracks with some nearly horizontal cracks. At the lower part of the column, horizontal cracks were generated due to the cyclic

changes in the loading direction. At drift ratios greater than 1.75%, parallel shear cracks were significant in the region of the beam parallel to the column and expanded to the axis of the beam and reached to its end. Likewise, the right joint first cracks appeared at lower and the upper beam-column interaction points at drift ratios 0.35% and 1.75%, respectively. As the test was presumed, those cracks continued to propagate until the end of the beam. Vertical inclined cracks on the sides of the column around its center began to appear at a drift level of 0.25% and propagated incrementally until a drift level of 1.25% was reached. Different from the left joint, the right one demonstrated mostly slanted cracks with some almost vertical cracks. At the lower part of the column also, horizontal cracks were generated due to the cyclic variations in loading. The cracks degradation in the zone of the beam opposite to the joint was major at drift ratios larger than 0.35% and spread towards the axis of the beam as drift level increased.

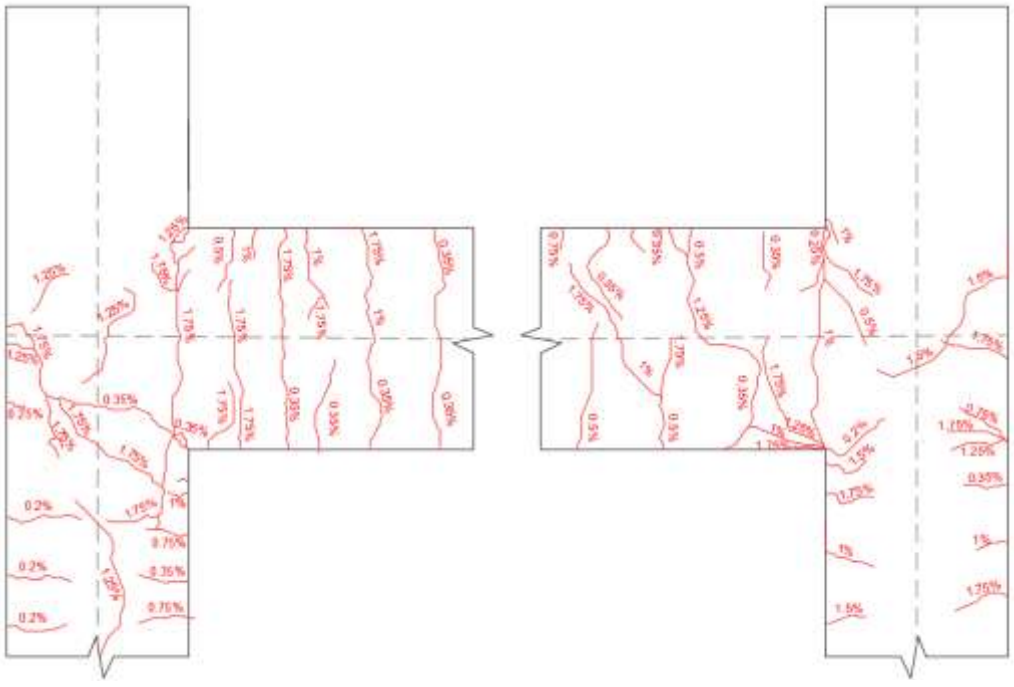

a) Left joint

b) Right joint

Figure 4.3 Crack pattern of the high ductile frame attributed with drift ratio at which the crack occurred

In the high ductile frame (Figure 4.3); however, the joint regions exhibited roughly more cracks than the low ductile one. At the left joint, the initial cracks were detected at the lower beam-column angle at a drift level of 0.35%. Moreover, initial cracks were detected during the first loading cycles at a drift level of 0.2% at the lower part of the joint perpendicular to the column cross-section. As the test proceeded, major cracks were developed parallel to the previously detected cracks at the other end of the column. When the load increased to the beginning crack value in the core region, cracks in the lower cross angle extended to the centerline of the columns and gradually widened. Vertical cracks first appeared at the beam bottom and then small cracks appeared at the middle of the beam at 1% drift and lastly propagated towards the other end as the drift increased. Similarly, at the right joint, the first cracks at the upper and lower beam-column angles were inspected at a drift level around 0.2% and 0.25%. During the reversal loading, major cracks and other small parallel cracks developed and expanded towards the centerline of the beam. The diagonal shear cracks in the frame were found at drift levels between 1% and 1.5%, becoming more recognizable at 1.75% when reached the beam axis. For drifts around 0.5% to 1.5%, slightly inclined vertical cracks started to emerge on the core of the column as well. At the lower part of the column, horizontal cracks were generated due to the reversal loading direction.

Since both samples exhibited almost identical crack patterns, it has been anticipated that the horizontal cracks happen to occur mostly at the joint region at the level of the bottom extended longitudinal reinforcement of the beam at a drift around 0.35% and subsequent drifts, could be attributed to the loss of bond between the reinforcing steel bars with the concrete and the structural steel column in that region. This may eventually lead to penetration of the longitudinal steel reinforcement of the beam into the joint core and slippage of the reinforcement with the consequent loss of capacity of the proposed composite connection. Nevertheless, notable diagonal cracks, which were gradually widened during loading, developed within all joint regions and were observed to be almost closed when unloaded. This is mainly due to the presence of structural steel sections in the columns which stiffened the frame and prevented the propagation of the diagonal cracks to the end of the columns. In other words, the joint

shear was adequately controlled by the structural steel sections rather than transverse reinforcement. As a result, the cracking pattern of both specimens implies that the degradation of the joint was predominantly correlated with the beam slipping of the longitudinal reinforcement, and the joint shear was properly governed by structural steel. Furthermore, as per the Turkish Earthquake Code (TEC 18), to ensure strong column-weak beam design, the resisting moment capacity of the columns was 1.32 greater than that of the beam resisting moment, and that can be apparently deduced from the creation of more cracks at the beam ends more than column ends.

4.2. Hysteretic Responses and Envelope Curves

Hysteresis loops demonstrate the evolution of lateral load versus beam-tip displacement (beam-column intersection) under reversal cyclic loadings associated with the yielding of transverse and longitudinal steel reinforcement in the members, the peak load of the joint, load-deflection envelope curve in the push and pull directions. The lateral load-deflection hysteretic loops of both specimens at each loading step are shown in Figure 4.4.

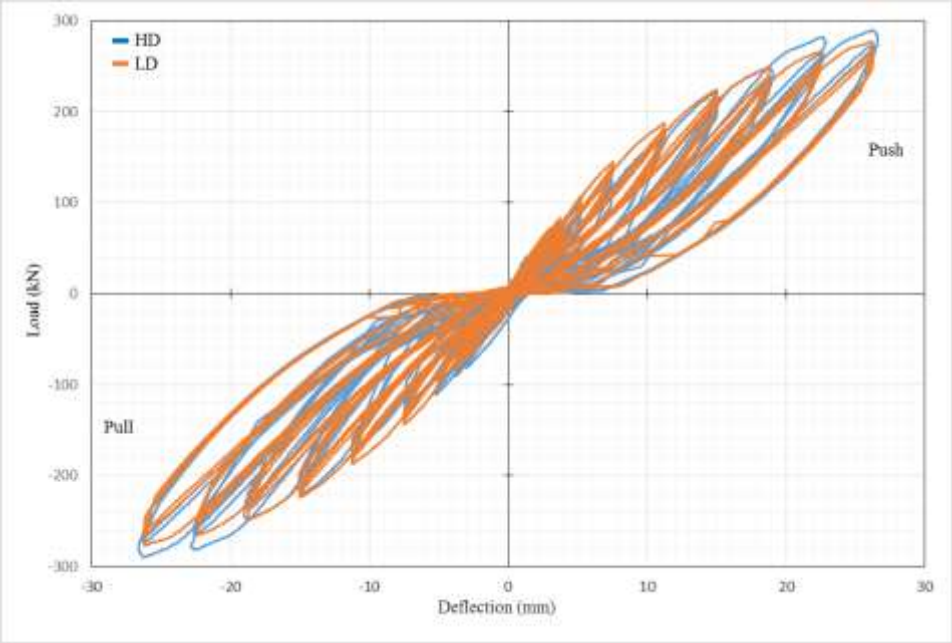

Figure 4.4 Load-deflection response (hysteretic loops)

Both specimens were tested up to a drift ratio of 1.75%, and they have nearly the same shape in the push and pull directions. However, there is a slight difference in the value of the maximum load reached in positive and negative directions at the same drift levels during the yield cycles, confirming that the presence of more transverse reinforcements in the joint region increases the strength of the frame. It may also be attributed to the steel reinforcement disposition and alignment or geometrical imperfections of the frames. As shown in Figure 4.4, no decline was observed in load-carrying capacity of both specimens up to the targeted drift 1.75%. The skeleton curve (Figure 4.5) was plotted using the peak load points associated with their deflection from each first cycle of each loading step of the hysteresis loops to indicate the characteristics of the structure. The symbols defined below in those figures represent the deformation of flexural steel reinforcement in the beam, yielding of longitudinal steel reinforcement in the beam, yielding of flexural steel reinforcement in the column, yielding of longitudinal steel reinforcement in the column and first crack in the specimens, respectively. As depicted in the envelope curve, the HD specimen experienced cracks on the concrete and yielding of reinforcement steel prior to the LD specimen. This might be due to the imperfections in the construction quality of each specimen.

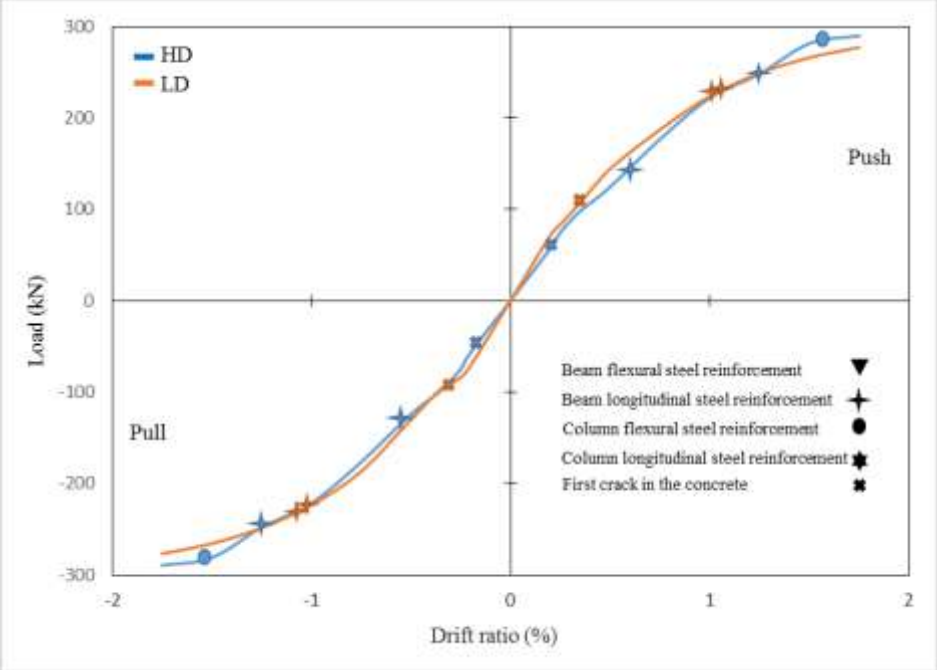

Figure 4.5 Load-drift ratio on skeleton curves of the tested specimens

4.3. Strain Profiles

The strain profile is the measured strains in the beam's longitudinal and transverse steel reinforcement bars as well as the column's longitudinal and transverse steel reinforcement bars, and the structural steel versus the drift ratio of both specimens and describing states at different stages of the drift (elastic and plastic stages). Strain profiles detected for both specimens were at push sets because the evolution of the strain was almost the same in the push and pull sets.

4.3.1. Low ductile frame

4.3.1.1. Strain profile in steel reinforcement of the beam

Both joints were almost identical in terms of strain evolution in the beam's reinforcement. As illustrated in Figure 4.6, the beam reinforcements managed to remain elastic up to a drift level of approximately 1.1%, and then yielded only at the beam lower longitudinal reinforcement of the left joint at the end (plastic hinge region) in the seventh loading step (i.e., at drift ratio of about 1.25%). However, the right joint witnessed the yielding of the upper steel reinforcement at a 1.70% drift level in the ninth loading step. The greatest strain value in the beam reinforcing steel was achieved at the maximum drift level of 1.75%, after which it declined to various extents when the load was released demonstrating the closure of the flexural cracks. The amount of strain of the lower reinforcement bars may best explain the multiple cracks developed at the lower part of the joint. Nevertheless, the remaining reinforcement kept behaving elastically until the end of the testing. It can be found from Figure 4.6 that the transverse steel deformation range at the end of the beam was the smallest because there was no loading on the beam (shear loading) except the axial loading induced from the lateral cyclic loading at the frame. The small deformations of transverse steel reinforcement in beams within the plastic hinge region are likely due to the small shear deterioration of concrete under cyclic loading. Considering strain profiles of both joints, it can be understood that the reinforcement bars of the beam had undergone different stresses and hence different yieldings. For instance, the beam upper rebars of the right joint experienced tension in the push set, while the lower ones experienced compression and the opposite occurred during the pull set.

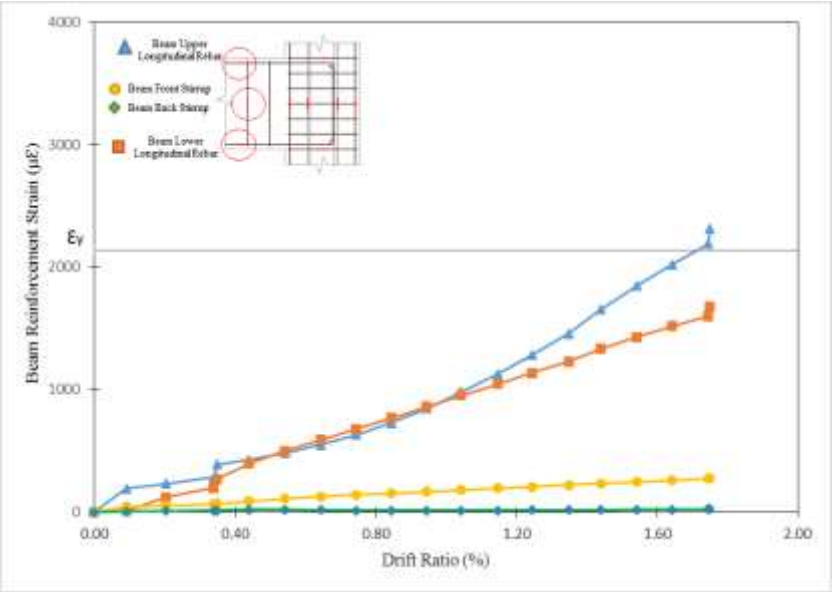

a) Right joint

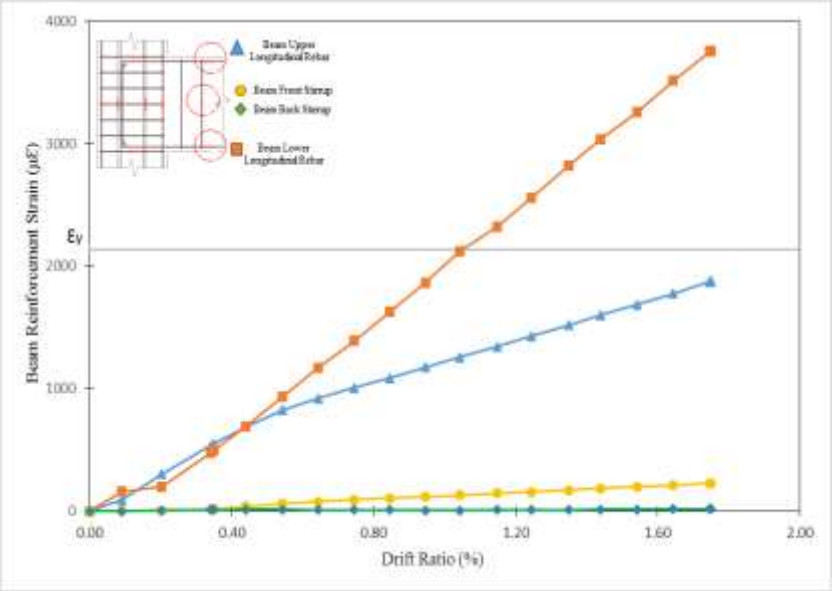

b) Left joint

Figure 4.6 Strain evolution in the beam reinforcement versus drift ratio

4.3.1.2. Strain profile in steel reinforcement and structural steel of the column

The column longitudinal steel bars and transverse steel reinforcement did not yield in the low ductile specimen (see Figure 4.7). The structural steel section also did not demonstrate even micro-strains, and that is due to the way it was aligned (strong axis positioned) inside the column. As a result of that, it was reasonable that the reinforcement of the column did not yield. However, the longitudinal reinforcement strain increased steadily before a 1.0% drift ratio, and then the inner rebar increased a bit faster than the outer one until the end of the test. Similarly, the transverse reinforcements of the column at the joint level deformed nearly identical. This observation implies that the column rebars, to some extent, made a minor contribution to the joint strength of the specimen compared to the structural steel that absorbed almost most of the load applied to the frame. Furthermore, the applied axial load may have an impact on decreasing the tensile strain that will be induced while applying the lateral reversal cyclic loading.

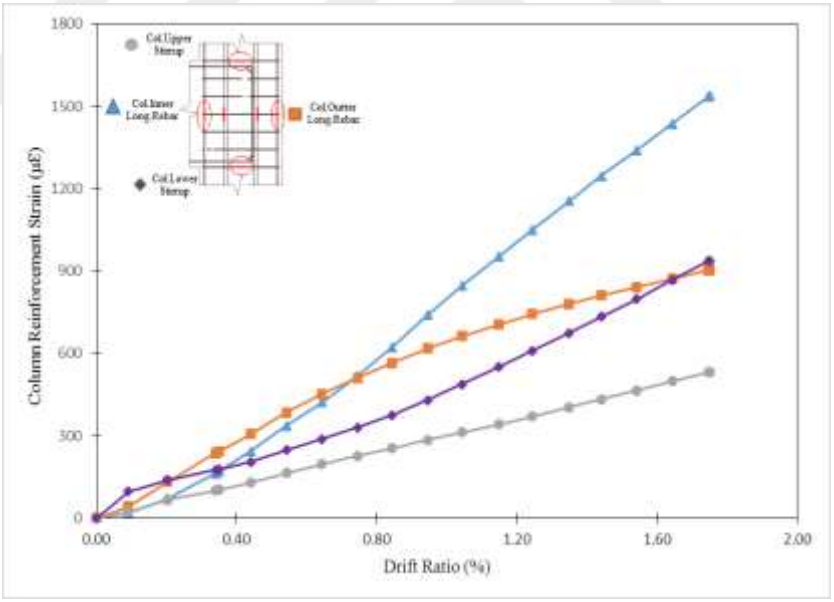

a) Right joint

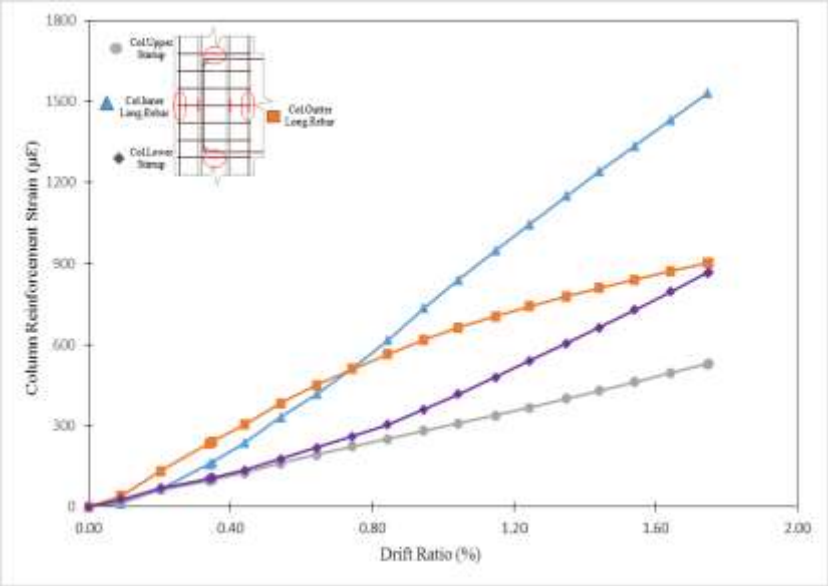

b) Left joint

Figure 4.7 Strain evolution in the column reinforcement versus drift ratio

4.3.2. High ductile frame

4.3.2.1. Strain profile in steel reinforcement of the beam

There are some significant differences in strain revolutions of the beam's longitudinal reinforcement between the right and left joints. Starting with the right joint (Figure 4.8), the beam upper longitudinal reinforcements behaved elastically up to a certain drift level and then yielded at the end of the beam (plastic hinge region) at drift level of about 0.53%. The greatest strain in the beam reinforcement bars was reached at the maximum drift level of 1.75%, after that it dropped when unloaded indicating the closure of the cracks. The yield of the upper reinforcement bars is the indicator of the cracks at the upper angle of the joint, yet the remaining reinforcement kept behaving elastically with minor deformations until the end of the loading. At the left joint, the lower longitudinal reinforcements yielded at a drift level of 1.75%, yet the transverse reinforcements remained elastic until the maximum reached drift with a very slow increase in the slope. Those minor deformations in transverse steel reinforcement of the beam within the plastic hinge region are likely due to the small shear deterioration of concrete under cyclic loading which was not loaded until failure. Not far from the behavior of the LD specimen, the strains of the upper and lower rebars of the beam in

both joints of the HD specimen experienced different stresses and that can best describe the difference observed in the behavior of both joints.

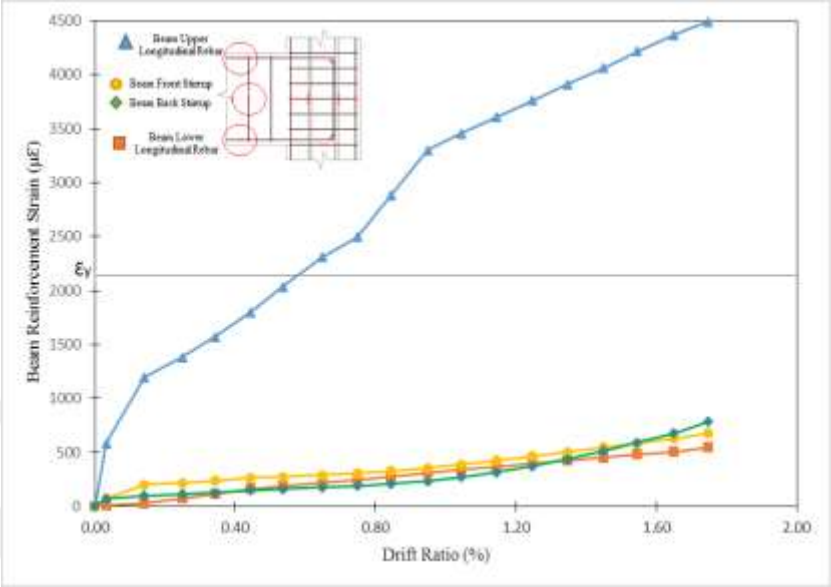

a) Right joint

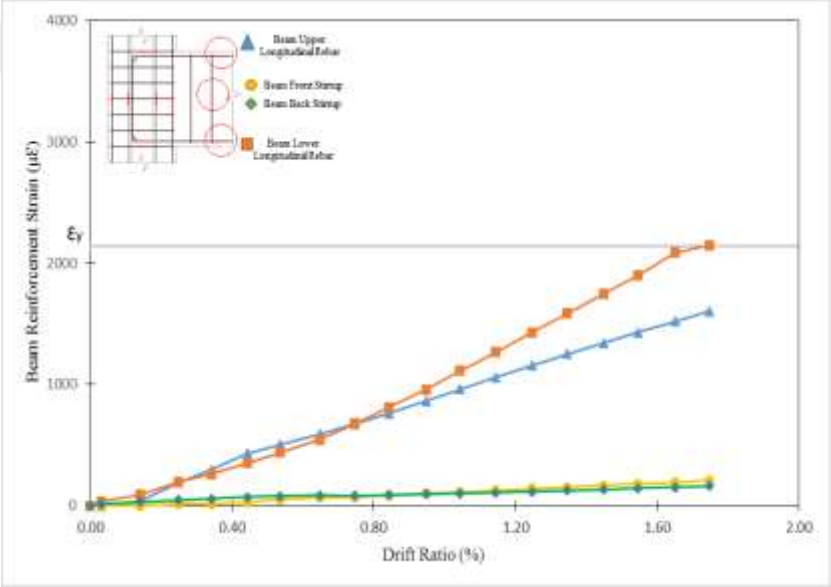

b) Left joint

Figure 4.8 Strain evolution in the beam reinforcement versus drift ratio

4.3.2.2. Strain profile in steel reinforcement of the column

The column steel reinforcement did not yield in the high ductile frame except the lower transverse steel reinforcement of the left joint (see Figure 4.9). It was stable throughout the testing until 1.55% drift level was attained, then it increased fastly. The structural steel section in both columns demonstrated very small micro-strains, and as mentioned previously that is due to its high strength and the way it was positioned inside the column. Nonetheless, the inner longitudinal reinforcement strain increased a bit faster than the outer one until the end of the test. As deduced previously in the low ductile specimen, it can be observed that the column reinforcement made a very small contribution to the joint strength of the specimen compared to the structural steel that absorbed almost most of the load applied to the frame.

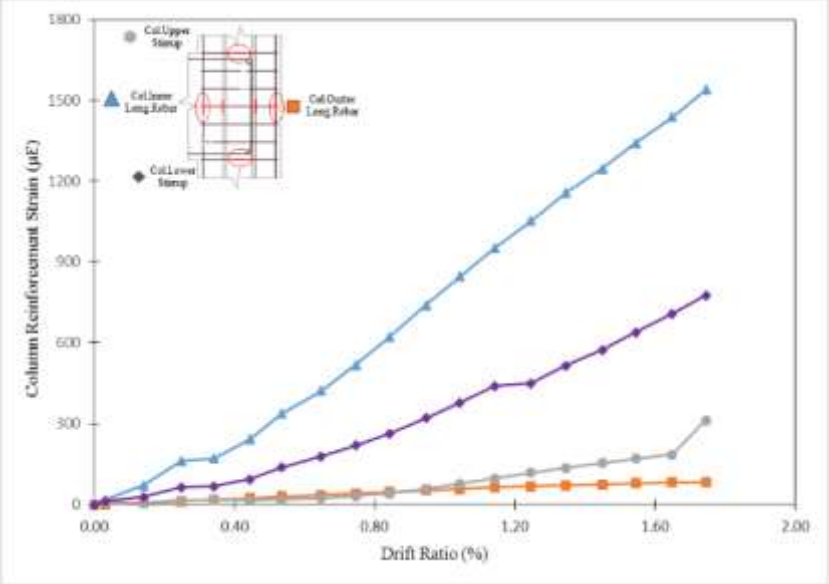

a) Right joint

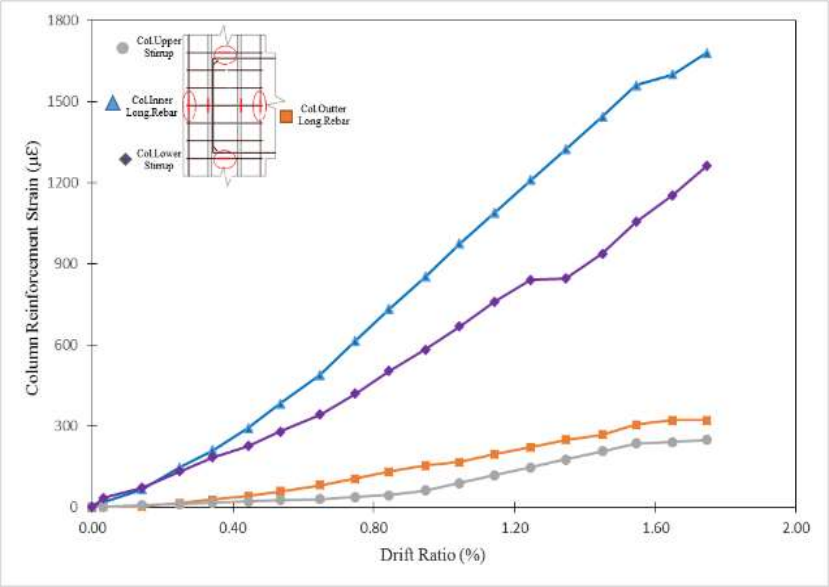

b) Left joint

Figure 4.9 Strain evolution in the column reinforcement versus drift ratio

4.4. Joint Shear Deformation

Shear deformation of the joint is the measure of the diagonal displacements within the joint region by a pair of LVDTs mounted above the joint panel that facilitated the calculation of joint shear deformation as shown in Figure 4.10. The total joint shear deformation can be computed by the following equation [21, 22]:

$$\gamma = \gamma_b + \gamma_c = \frac{\sqrt{h_b^2 + h_c^2}}{2h_b h_c}(\Delta_I - \Delta_{II}) \tag{4.1}$$

Here, γ_b and γ_c are the joint shear strain at beam side and column side, and h_b and h_c are the height and width of the joint core, and Δ_I and Δ_{II} are the deformations measured by LVDTs I and II.

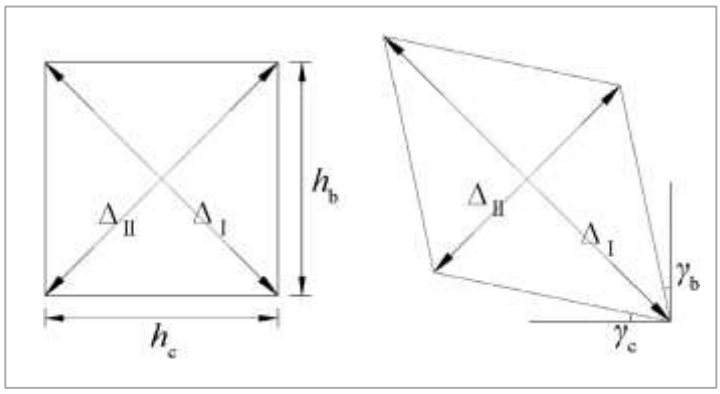

Figure 4.10 Beam–column joint area deformation[25]

The maximum joint shear strains calculated in the positive and negative loadings at the last cycle are $+5.89\times10^{-4}$, -3.31×10^{-4} rad for the right joint and $+1.05\times10^{-3}$,-1.05×10^{-3} rad for the left joint of the low ductile specimen, while the maximum joint shear strains for the right joint and left joint of the high ductile specimen are $+6.25\times10^{-4}$, -2.38×10^{-4} rad and $+3.84\times10^{-3}$, -9.96×10^{-4} rad, respectively. The positive sign refers to the lengthening and negative sign refers to the shortening of the joint diagonals. Even though loading protocol used in the test for the frame from both sides is the same in all cycles, the shear deformation determined in both specimens were slightly greater in the push (positive direction) than that in the pull (negative direction). Both test specimens exhibited similar shear deformation responses with relatively smaller values before a drift ratio of 0.5%, but their deformation responses then gradually increased until it reached the maximum at the drift level 1.75% because the main damages were focused on the beam-column region. As soon as the cracks began to propagate at the end of the beam, they reduced the confinement to the joint region provided by the beams, and further reduced the shear stiffness of the joint region. It can be concluded that, if the number of loading cycles adopted had increased until the ultimate capacity of the joints, the shear deformations of the joints of both specimens would increase, and the discrepancy of joint shear deformations between LD and HD specimens would be larger than the obtained one.

4.5. Energy Dissipation

Fundamentally, the survival of the structural system in an earthquake depends on its capability to dissipate energy. The energy dissipation can be estimated by adding up the energy dissipated during each load-deflection cycle throughout the test, which is the area enclosed by each hysteretic loop. Figure 4.11 illustrates the progression of the cumulative energy dissipation with the drift ratio.

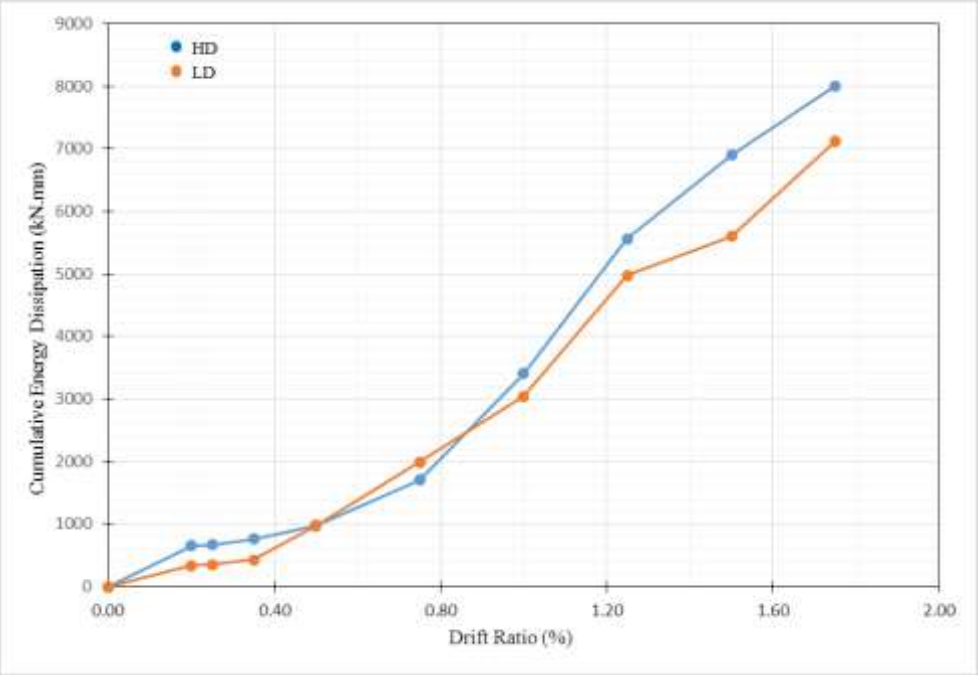

Figure 4.11 Cumulative energy dissipation vs. drift ratio

Energy dissipation is primarily due to plastic deformation of the reinforcing steel, concrete and its interface and also the slips between structural steel and concrete. It is obvious that the high ductile specimen achieved more energy dissipation, while the low ductile specimen exhibited less energy dissipation capacity, which started to be noticeable at 1.25% drift. It can be concluded that the increase in the transverse reinforcement ratio oriented along the column at the joint region exhibited higher flexibility and hence dissipated larger amount of energy, which is favorable. The exitance of more parallel horizontal shear cracks in the HD specimen than that of the LD specimen may describe the effectiveness of using more transverse reinforcement at the joint region.

4.6. Stiffness Degradation

The experimental stiffness values were calculated for both frames based on the peak-to-peak secant stiffness principle [26]. Cyclic stiffness is defined as the slope of the line connecting the peak loads in the positive and negative directions of loading during the first repeat of each loading cycle.

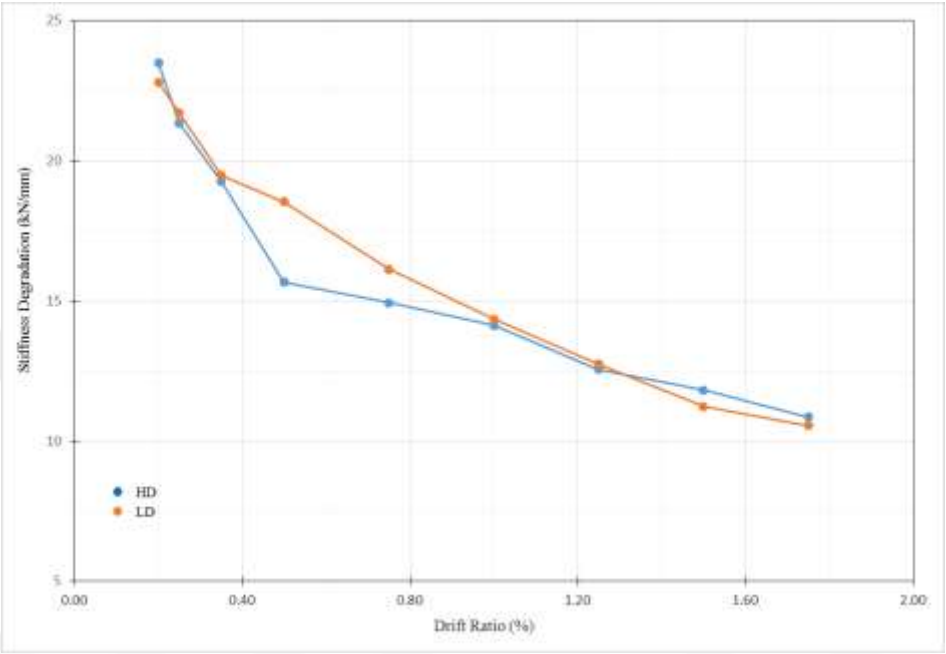

Figure 4.12 Stiffness degradation for the tested specimens (first repeat)

As presented in Figure 4.12, both specimens displayed similar pre-yield degradation patterns in secant stiffness between 0.2% and 0.35%. After then, the low ductile specimen exhibited considerably higher secant stiffness values compared to those in the high ductile specimen up to a drift level of 1%. This difference, however, decreased as the drift ratio increased in the following cycles until the end of testing as illustrated in Table 4.3. In view of the above, it might be concluded that the secant stiffness values of these two specimens were averagely close to each other due to the existence of structural steel sections that were primarily stiffening the frame. However, It is noteworthy that the increase in the transverse reinforcement ratios of the SRC column might not have a large impact on the stiffness because the secant stiffness values of these two specimens were interchanging throughout the testing.

Table 4.3 The average difference between the HD and LD stiffness degradation

Drift (%)	Average Difference (%)
0.20	3.00%
0.25	1.69%
0.35	1.14%
0.50	18.34%
0.75	7.96%
1.00	1.54%
1.25	1.54%
1.50	4.97%
1.75	2.89%

CHAPTER 5

CONCLUSIONS AND RECOMMENDATIONS

5.1. Summary

This thesis presents a detailed investigation of the seismic effectiveness and fundamental behavior of steel-concrete composite joints. It focuses particularly on steel-concrete composite frames with two reinforced concrete-encased steel (SRC) columns and one connecting reinforced concrete (RC) beam. Correspondingly, two scaled-down composite frames were designed, constructed, instrumented, tested and lastly examined to identify the impacts of several percentages of column reinforcement bars on joint performance, and to investigate any potential impact on shear strength. The specimens were tested under constant concentrically applied axial loading on top of the columns, and varied lateral displacement-controlled reversal cyclic loading applied on one side of the frame specifically at the region of intersection between the beam and the column. The test parameters were column transverse reinforcement ratio, joint aspect ratio, lateral reversal cyclic load, and the axial load.

5.2. Conclusions

Based on the findings of the experimental study carried out and presented in this manuscript and within the set of parameters evaluated, the primary outcomes and observations of this investigation are listed hereafter.

1. At drift ratios between 0.2% and 0.35%, the difference between the stiffnesses of both specimens did not exceed 3%. From this value of drift ratio (0.35%), the rate of stiffness degradation for HD specimen decreased significantly until a drift level of 0.75%, and then the HD specimen, exhibited stiffness degradation with a similar trend to LD specimen. As a result, the increase in

the transverse reinforcement ratios of the SRC column might not have large impact on the secant stiffness.

2. The increase in the transverse reinforcement ratio oriented along the column at the joint region exhibited higher flexibility and hence dissipated larger amount of energy.
3. Based on the strains observed in the longitudinal and transverse steel reinforcements in the columns and joint region, the column rebars, to some extent, made a minor contribution to the joint strength of the specimen compared to the structural steel that absorbed almost all of the load applied to the frame.
4. For the composite frame designed in this study, the RC beam finally suffered from bending shear failure, and the plastic hinge appeared first in the beam and then in the column, which illustrates that the failure mechanism of the SRC column - RC beam frame structure results firstly from beam hinge failure.
5. The joints were stiffened by the steel section and were not damaged seriously from beginning to end. Therefore, the frame is characterized by the concept of "strong joint, strong column, and weak beam".
6. From the hysteresis loops, in the load-carrying capacity and energy dissipation capacity points of view, the seismic performance of the high ductile frame reported in the existing study is superior to that of the low ductile frame under the same parametric conditions.
7. It can be concluded from this study that the SRC column–RC beam frames employing extra column reinforcements ratio have better seismic performance.

5.3. Recommendations Future Research Work

Additional research studies are needed for the investigation of composite frames. The recommendations for further investigations are stated as follows:

1. Simulation of the proposed frames using finite element software and performing nonlinear dynamic analyzes is required to identify the impacts of joint behavior and failure on the overall performance of the building.

2. Perform further beam-column joint tests of proposed composite systems that are continued to somehow evaluate the developed failure models until lateral failure.
3. Extend the models fabricated in the current study to the interior, intermediate, and exterior joints to investigate the effect of the joint location on the seismic performance of the proposed joints.
4. The composite models in the current study are addressing exclusively the square SRC columns. Further investigations are recommended to produce similar models for circular columns due to the disparity in the stability of sections and concrete containment between the two mentioned configurations.
5. The effect of various types of connections and techniques of connecting the beam reinforcement bars to the column (welding or anchoring of steel bars of the beam with structural steel of the column) can be further studied.
6. The influence of the different structural parameters that are not considered in this study can be thoroughly evaluated. For instance, the effect of shear studs welded in structural steel on the shear strength of the developed joint. Such a detailed understanding is essential for implementing a full-range shear force-slip relationship between shear studs and concrete. Moreover, parameters of concern should also involve the influence of the loading history on shear and axial strength and drift capacity in terms of the number of cycles.
7. Datasets available on steel-concrete composite frames (including SRC columns to RC beams) are relatively limited. As a consequence, more tests should be carried out, so that they can be used as benchmark models for advanced analysis of composite frames.

REFERENCES

[1] Skyscraper Center, “2019 Tall Building Year in Review,” 2019. [Online]. Available: http://www.skyscrapercenter.com/year-in-review/2018. [Accessed: 03-Dec-2019].

[2] S. Peng, C. Xu, C. Wang, and Z. Ma, “Influence of the degree of damage and confinement materials on the seismic behavior of RC beam-SRC column composite joints,” *Compos. Struct.*, p. 34, 2019.

[3] ABAQUS, “Computer-Aided Engineering,” 2018.

[4] D. Ma, L. H. Han, and X. L. Zhao, “Seismic performance of the concrete-encased CFST column to RC beam joint: Experiment,” *J. Constr. Steel Res.*, Vol. 154, pp. 134–148, 2019.

[5] C. Xu, S. Peng, J. Deng, and C. Wan, “Study on seismic behavior of encased steel jacket-strengthened earthquake-damaged composite steel-concrete columns,” *J. Build. Eng.*, Vol. 17, pp. 154–166, 2018.

[6] L. Xie, D. Zhao, G. Li, “Test and parametric analysis of postfire seismic performance of SRC column–RC beam joints,” in *Proceedings of the international conference on civil, architecture and environmental engineering*, pp. 135–138, 2016.

[7] J. Kong, Y. Zou, C. Li, and Z. Wan, “Nonlinear numerical analysis of SRC Frame end Joint,” *Adv. Mater. Res.*, Vol. 755, pp. 1151–1155, 2013.

[8] W. P. Jacobs V and J. F. Hajjar, “Load transfer in composite construction,” *Struct. Congr.*, pp. 1229–1240, 2010.

[9] J. F. Hajjar, “Composite steel and concrete structural systems for seismic engineering,” *J. Constr. Steel Res.*, Vol. 58, pp. 703–723, 2002.

[10] S. Shin, J. Kim, and J. Ahn, “Transverse reinforcement of RC columns considering effective lateral confining reduction factor,” *J. Asian Archit. Build.*

Eng. ISSN, Vol. 7581, pp. 501–508, 2018.

[11] R. L. Ã. Vollum and J. B. Ã. Newman, "Strut and tie models for analysis/design of external beam ± column joints," No. 6, 1999.

[12] P. G. Bakir and H. M. Boduroğlu, "A new design equation for predicting the joint shear strength of monotonically loaded exterior beam-column joints," *Eng. Struct.*, Vol. 24, No. 8, pp. 1105–1117, 2002.

[13] ACI Committee 374, "Guide for testing reinforced concrete structural elements under slowly applied simulated seismic loads (ACI 374.2R-13)," *Am. Concr. Institute, Farmingt. Hills, MI*, p. 22, 2013.

[14] C. Clyde, C. P. Pantelides, and L. D. Reaveley, *Performance-based evaluation of exterior reinforced concrete building joints for seismic excitation*. Pacific Earthquake Engineering Research Center, College of Engineering …, 2000.

[15] M. Barnes, S. Jigorel, and S. Park, "Exterior non-ductile beam-column joints," 2008.

[16] S. Pantazopoulou and J. Bonacci, "Consideration of questions about beam-column joints," *Struct. J.*, Vol. 89, No. 1, pp. 27–36, 1993.

[17] R. L. Vollum, "Design and analysis of exterior beam-column connections." PhD Thesis, 1998.

[18] Y. Kurose, G. N. Guimaraes, Z. Liu, M. E. Kreger, and J. O. Jirsa, "Study of RC beam-column joints under uniaxial and biaxial loading," *Rep. No. PMFSEL 88*, Vol. 2, 1988.

[19] F. J. Vecchio and M. P. Collins, "Modified compression-field theory for reinforced concrete elements subjected to shear," *Journal of the American Concrete Institute*, Vol. 83, No. 2. pp. 219–231, 1986.

[20] AISC, "Specification for Structural Steel Buildings," pp. 1–612, 2010.

[21] TEC18, "Turkish Earthquake Code," *Turkish Minist. Public Work. Hous.*, 2018.

[22] P. by I. N. reproduction or networking permitted without license from IHS, *ACI*, Vol. 11. 2005.

[23] C. W. Beckingsale, “Post elastic behavior of reinforced concrete beam-column joints,” University of Canterbury, 1980.

[24] B. Chang, T. Hutchinson, X. Wang, and R. Englekirk, “Seismic performance of beam-column subassemblies with high strength seismic performance of beam-column subassemblies with high-strength steel reinforcement,” *ACI Struct. J.*, Vol. 111, p. 10, 2014.

[25] H. Yang, W. Zhao, Z. Zhu, and J. Fu, “Seismic behavior comparison of reinforced concrete interior beam-column joints based on different loading methods,” *Eng. Struct. J.*, Vol. 166, pp. 31–45, 2018.

[26] S. Alavi, D. Mostofinejad, and P. Alaee, “Effects of high-strength reinforcing bars and concrete on seismic behavior of RC beam-column joints,” *Eng. Struct.*, Vol. 183, 2018, pp. 702–719, 2019.